OSLOMET

ACCESSIBILITY
Reserved for 3 years

OSLO METROPOLITAN UNIVERSITY
STORBYUNIVERSITETET

Master's Degree in
Structural Engineering and Building Technology
Department of Civil Engineering and Energy Technology

MASTER THESIS

THESIS TITLE	**DATE**
Ballistic impact on concrete plates with compressive strengths of C35, C75 and C110	15.06.2020
	NUMBER OF PAGES
	82
AUTHOR	**SUPERVISORS**
Desmond Veerakathy	Mahdi Kioumarsi Martin Kristoffersen

IN COLLABORATION WITH	**CONTACT PERSON**
Norwegian Public Roads Administration and NTNU	Kjersti Kvalheim Dunham

SUMMARY

The main objective of this thesis has been to assess the behavior of concrete plates subjected to ballistic impact from ogival steel projectiles. The experiments were run at the Structural Impact Laboratory (SIMLab) at NTNU, where high-velocity projectiles were fired at concrete plates with compressive strengths of C35, C75 and C110. The Recht-Ipson model and the CEA-EDF perforation limit formula were used and compared with the experimental results. The results showed that the ballistic limit velocity increased by about 16% from concrete C35 to C110.

Evaluation of existing numerical simulations showed that it is possible to predict the residual velocity of the projectiles from the ballistic impact test by using the original HJC model, the modified HJC model and the JH-2 model. These material models can provide adequate results compared to the experimental results.

Investigation of ethical issues related to the experimental work showed that civilian research projects with interest to the military may cause several ethical issues. Refraining from the research is probably the only way of avoiding any possibility of military applications. Since the issues are complicated, it is not possible to make a statement of what is and is not ethical.

3 KEYWORDS
Experimental method
Ballistic impact
Concrete plates

Abstract

The main objective of this thesis has been to assess the behavior of concrete plates subjected to ballistic impact from ogival steel projectiles. The experiments were run at the Structural Impact Laboratory (SIMLab) at NTNU, where high-velocity projectiles were fired at concrete plates with compressive strengths of C35, C75 and C110. The Recht-Ipson model and the CEA-EDF perforation limit formula were used and compared with the experimental results. The results showed that the ballistic limit velocity increased by about 16% from concrete C35 to C110.

Evaluation of existing numerical simulations showed that it is possible to predict the residual velocity of the projectiles from the ballistic impact test by using the original HJC model, the modified HJC model and the JH-2 model. These material models can provide adequate results compared to the experimental results.

Investigation of ethical issues related to the experimental work showed that civilian research projects with interest to the military may cause several ethical issues. Refraining from the research is probably the only way of avoiding any possibility of military applications. Since the issues are complicated, it is not possible to make a statement of what is and is not ethical.

Acknowledgements

This master thesis was carried out in cooperation with OsloMet, NTNU and Norwegian Public Roads Administration (NPRA). I acknowledge NPRA for financial support considering the experiments at NTNU in Trondheim, and for giving me this opportunity to work with researcher and external supervisor Martin Kristoffersen from NTNU. I would also like to thank my internal supervisor Mahdi Kioumarsi's engaging guidance through the thesis with excellent and useful feedback. I also recognize Stian Ausland who participated in the literature review.

It would not have been possible to complete this thesis without help and support from many people.

A special thanks to Kjersti Kvalheim Dunham who made this thesis possible as the former project leader of ferry free E39.

To my fellow students at OsloMet, thank you for your great friendships, which made my master's degree more than just a time of studying.

Certainly, my deepest and greatest appreciation is reserved for my beloved parents and grandmother who supported and encouraged me through all these years. They allowed me to study hard and achieve goals they never had the chance to achieve themselves. I wish to express my sincere appreciation to my little brother, for his endless love and incredible support throughout my entire life.

Finally, I would like to thank my love, Thu Huong. She was always there to cheer me up and stood by my side through all the good and bad times.

Contents

List of figures

List of tables

Nomenclature

Abbreviations

$CaCO_3$	*Calcium carbonate*
CaO	*Calcium oxide*
CO_2	*Carbon dioxide*
FEM	*Finite Element Method*
HJC	*Holmquist-Johnson-Cook material model*
MHJC	*Modified Holmquist-Johnson-Cook material model*
NPRA	*Norwegian Public Roads Administration*
SFTB	*Submerged Floating Tube Bridge*
SIMLab	*Structural Impact Laboratory at NTNU*
w/c ratio	*Water-cement ratio*

Greek letters

$\left(\varepsilon_p^f\right)_{MIN}$	*Minimum plastic strain to fracture*
α_{HJC}	*Damage constant in MHJC and HJC, Courant number in explicit time integration, material parameter for concrete tensile strength*
β_{HJC}	*Damage parameter in MHJC and HJC*
ε_p^f	*Plastic strain at fracture*
$\tilde{\varepsilon}_{pl}$	*Equivalent plastic strains*
$\dot{\varepsilon}$	*Total strain rate*
$\dot{\tilde{\varepsilon}}_{pl}$	*Equivalent plastic strain rate*
$\dot{\varepsilon}_{pl}$	*Plastic strain rate tensor*
μ	*Friction coefficient, volumetric strain*
μ_{crush}	*Volumetric strain when the concrete starts to get crushed*
μ_{lock}	*Volumetric strain when the air voids has collapsed totally*
σ	*Stress matrix*
ρ	*Density*
ρ_0	*Initial density (Concrete density)*
ρ_c	*Concrete density*
σ'_I, σ'_{II}, σ'_{III}	*Ordered principal stresses*
σ'_I	*Stress tensor*

σ_Y	*Yield stress*
$\sigma_1,\ \sigma_2,\ \sigma_3$	*Diagonal stress components of the 3 × 3 stress matrix*
σ_{eq}	*Equivalent stress*
σ_H	*Hydrostatic stress*
$\sigma_I,\ \sigma_{II},\ \sigma_{III}$	*Ordered principal stresses*
$\overline{\sigma}$	*Effective stress tensor*
$\overline{\sigma}_{eq}$	*Equivalent von Mises stress of the effective stress tensor*
θ	*Deviatoric polar angle*
φ	*Yield function*

Roman letters

A	*Normalized cohesive strength in HJC model*
a	*Material constant in the Recht-Ipson model*
B	*Normalized cohesive strength in HJC model*
C	*Strain rate parameter*
D	*Damage parameter*
D_C	*Compaction damage*
D_S	*Shear damage*
D_T	*Tensile damage*
e	*Shape factor describing out-of-roundness of the yield surface*
$F\left(\dot{\varepsilon}_{eq}^{*}\right)$	*Strain rate influence in the MHJC material model*
h_e	*Characteristic element size*
$\boldsymbol{I}$	*Identity matrix*
I_σ	*First principal stress invariant*
$i_{\overline{r}}$	*Scaled specific impulse*
i	*Increment number*
J_2	*Second principal stress invariant of the deviatoric stress tensor*
K_Ω	*Non-local variable*
L	*Lode parameter*
l	*length scale*
M	*Consistent matrix*
m_{pl}	*Plug mass*
m_p	*Projectile mass*

N	*Pressure hardening exponent in HJC and MHJC material model*
n	*Step number*
P_0	*Ambient pressure*
P_{SO}	*Maximum overpressure caused by the blast*
P	*Pressure*
P^*	*Normalized pressure*
P_{crush}	*Pressure where crushing of concrete starts*
P_{lock}	*Pressure where air voids are fully collapsed*
p	*Material constant in the Recht-Ipson model*
Q	*Heat flow*
R^{ext}	*Applied load vector*
R^{int}	*Internal load vector*
$R(\theta, e)$	*MHJC reduction of the shear strength on the compressive meridian*
r	*Global nodal displacement vector*
$\ddot{r}$	*Global nodal acceleration vector*
$\dot{r}$	*Global nodal velocity vector*
S_{max}	*Normalized maximum strength that can be developed in the HJC and MHJC material model*
s_c, s_t	*Stress state functions applied to represent stiffness recovery effects*
T	*Maximum principle stress in tension the material can support, stress triaxiality in the HJC and MHJC material model*
T^*	*Normalized tensile strength in the HJC and MHJC material model*
V	*Volume*
v	*Velocity*
v_{bl}	*Ballistic limit velocity*
v_i	*Initial velocity*
v_r	*Residual velocity*
W_{free}	*Work done in an elastic impact with a plug free from the plate*
W_{shear}	*Shear work done in the shear zone around the plug periphery*

Chapter 1 - Introduction

The Norwegian Public Roads Administration is working on an extensive research project to replace all ferry connections along the coastal highway E39 route along the west coast of Norway. The route goes from Kristiansand to Trondheim, and the ferry connections are considered replaced with fixed connections in the form of bridges and tunnels. Different design concepts are evaluated for the bridges and tunnels, and one of the evaluated concepts is the Submerged Floating Tube Bridge (SFTB), which is a tube construction made of concrete. The reason why it is called a bridge, and not a tunnel, is because it is a construction. Two different anchoring concepts are considered for the SFTB: one concept with floating pontoons, and one concept with tethers. The use of tethers anchored to the ground is a more expensive solution, and the anchoring system needs to be maintained a lot to be secure against hazardous occurrence. The anchoring concept with pontoons seems to be the most feasible one.

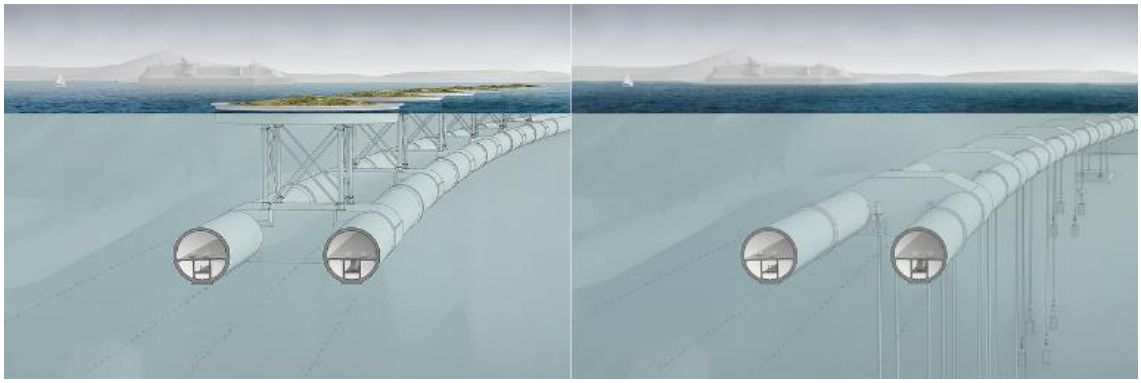

Figure 1: Illustration of SFTB with pontoons and tethers [1].

An internal explosion and fire from accidents involving tankers transporting dangerous cargo, e.g., liquid natural gas or gasoline, or from a potential terrorist attack could cause extreme destructions if the concrete is not strong enough to withstand the loads [2]. In the worst case, water can penetrate due to cracks, and the tube itself can break down. It is therefore essential to examine the behavior of concrete under extreme load conditions, and how the material can be strengthened as best as possible.

Concrete plates of C35, C75 and C110 are tested against impact from steel projectiles in the compressed gas gun facility at SIMlab for the assessment of their ballistic limit curves, and to see how concrete plates behave when subjected to an ogival steel projectile. An explosive detonation gives rise to blast pressure and fragments, and shock loads induced

by the shock wave. In this thesis the focus is only on the fragments, where the projectiles used in the experiments represent the fragments.

The finite element analysis is a method of numerically solving a range of problems, and that is appropriate to use in complex processes such as ballistic impact on concrete. The numerical method is widely used and allows virtual tests using mathematical models. A literature review of numerical simulations is conducted focusing on three material models: The Original Holmquist-Johnson Cook, the Modified Holmquist-Johnson Cook and the JH-2. This is done to verify that the material models have a useable ability to predict experimental results.

Ethical considerations are discussed to highlight the importance of understanding possible issues of experimental work. A central part is about dual use, which is associated with military involvements, because the field is essential to both civilian and military applications.

1.1 Objectives

The overall objective of this thesis is to find out how concrete plates with compressive strengths of C35, C75 and C110 behave under ballistic impact. The following specific objectives were identified:

- To evaluate existing numerical simulations to predict the response of concrete plates subjected to ballistic impact.
- To investigate how concrete strength affects the ballistic limit.
- To investigate how the Recht-Ipson model and the CEA-EDF perforation limit formula are used to describe the experimental results.
- To investigate ethical issues related to the experimental work.

1.2 Scope and limitations

The experiments are conducted in the compressed gas gun facility at NTNU, where each concrete plate is struck by an ogival steel projectile. The Recht-Ipson model is used to achieve an analytical approach to the results of the experiments. The literature review is focusing on existing literature with a scope of increasing the knowledge of the ballistic impact on concrete as a material. Numerical simulations are discussed as a method to verify the experimental results.

The limitations of this thesis are summarized as follows:

- The research deals with observational study by analyzing the recorded videos from the experiments during perforation of each concrete plate to determine initial and residual velocity. The conducted experiments focus only on the fragments from an explosion, and not the blast pressure and shock loads.
- The Recht-Ipson model is used to analyze and determine the ballistic limit curve for concrete plates with compressive strengths of C35, C75 and C110.
- Opportunities with numerical simulations are presented through the work of others, but no simulations have been carried out in this thesis.

1.3 Outline of the thesis

This thesis consists of eight chapters. A brief description of each chapter is given as follows:

Chapter 1 includes the introduction, objective, scope and limitations of the work. *Chapter 2* deals with the background of this thesis including knowledge about concrete, ballistic impact, finite element method, material models and numerical simulations of ballistic impact problems. *Chapter 3* describes the methodology and experiment used in this study. *Chapter 4* presents the analysis of the experimental results. *Chapter 5* describes the ethical challenges associated with this topic. *Chapter 6* deals with the discussion of the preceding chapters. *Chapter 7* summarizes the conclusions, and finally, suggestions for future work are given in *Chapter 8*.

Chapter 2 - Background

Impact studies have been a research topic for decades, and substantial effort is spent to understand the physical part happening under ballistic penetration [3-8]. The penetration process has also been described mathematically. Back in the days, most of the studies were performed experimentally. Many analytical models have been proposed over the years, but the impact events bring complexity that limits the general use of analytical models [9-11]. Nowadays, more of the progress is performed numerically with finite element method adopted as a known tool in most communities. However, numerical simulations do not have the accuracy and robustness required for reliable material description during perforation [12].

There is a need of more knowledge when it comes to the impact phenomenon on concrete as a material. Concrete is a complex material consisting of different materials such as cement, aggregates and water. That makes the material more unpredictable than isotropic materials such as steel. Lots of experiments must be completed to determine its behavior.

The background theory consists of knowledge of concrete material, ballistic impact, finite element method, material models and a review of existing numerical simulations of ballistic impact problems.

2.1 Concrete

Concrete as a material has become an extensively used material in structural engineering. Concrete is a very complex and somewhat unclear material. All sub-materials are local and have a broad range of properties. This makes it very difficult to predict the properties of the concrete. It is, therefore, essential to have a general knowledge of how sub-materials and mixing conditions affect the material structure of the concrete, and how it controls the material properties [13]. The material has a tensile strength of about 1/10 of the compressive strength, and that is the reason why concrete used in buildings and other engineering applications is reinforced with steel. Therefore, it is difficult to predict the behavior of concrete compared to ductile and isotropic metals like steel and aluminum. Concrete is widely used in the world, and in Norway, the yearly consumption of concrete is about 1.5 million tons [14]. This contributes to the overall CO_2-emissions, and much research has been performed to reduce the CO_2-emissions and spare the environment.

2.1.1 Structural properties of concrete

Concrete is a mix between water, matrix (cement paste) and aggregates. It is also normal to use admixtures and mineral additives [14]. The aggregates make up approximately 70% of the concrete, while cement, water, admixtures and mineral additives make up approximately 30% [13]. Another component of the concrete structure is the transition zone, which is an interface between the aggregates and cement, which is also present in cured concrete [15, 16]. The binding properties in concrete are caused by the hydration process where cement reacts with water. The strength depends on the water-cement (w/c) ratio as it influences the hydration process.

The transition zone is responsible for the concrete being much weaker in tension than in compression. The existing cracks from the pores do not take much load in tension before they start to expand, but in compression, the pores are not extended as easily.

The aggregate gives the main weight and the elastic modulus of the concrete [15]. The aggregate consists of small stones and larger rocks and differs a lot in size, shape and texture. Together with the volume of aggregate, it is essential for the concrete's properties. Larger aggregate sizes increase the need for a higher w/c ratio, which in turn increase the number of pores in the transition zone, and thus the strength of the concrete is reduced. It is, therefore, essential to have a varying amount of aggregates based on size, shape and texture.

Cement is an excellent pulverized material consisting of limestone, silica, alumina and iron oxide. There are many types of cement, and the most common type is Portland cement. Cement works as a binder but does not gain these properties before it reacts with water in the hydration process [15]. Reduction of limestone reduces the CO_2, where the calcination process in the kiln directly releases CO_2 and contribute with approximately 50% of the cement's total CO_2-emissions. This is understandable from the chemical equation of the calcination below:

$$CaCO_3 \rightarrow CaO + CO_2 \qquad (2.1)$$

where $CaCO_3$ is the chemical composition of calcium carbonate (limestone) and CaO is the chemical composition of calcium oxides (burnt lime). Reducing the amount of limestone in the cement will have a positive effect on the total CO_2-emission. The cement

itself dominates the carbon footprint and accounts for more than 90% of the total carbon footprint for concrete [13]. Pozzolans as silica fume and fly ash can be added to the cement and thus reduce the amount of limestone, which reduces the CO_2-footprint from the cement. The pozzolans are by-products from coal industry (fly ash) and silicon productions (silica fume) and other industry (other pozzolans). It is, therefore, very fortunate to use this in concrete.

During the hydration process cement reacts with water, which increases strength and density. The rate of hydration decreases with time, and after 28 days the concrete is assumed to have reached the maximum strength, even though concrete strength usually increases further after 28 days. The pH-value increases during the hydration process as the alkalis in the cement dissolve in the water [14]. The hydration process is sensitive to temperature and depending on it. Norwegian Standard EN 12390-2 [17] describes that the test specimens should be cured in a chamber with a temperature of about 20˚C and high humidity of more than 95% or submerged in water. Lower temperatures will slow down the hydration process, and if the humidity is lower, the concrete may not reach the maximum potential strength.

The water-cement ratio plays a crucial role in the concrete properties and strength. The w/c ratio tells something about the number of liters of water per kilo of cement. The cement reacts under the hydration process with 40% of the weight of cement paste, which means that the w/c ratio is equal to 0.4. The higher w/c ratio results in reduced concrete strength because the pores in the concrete increase. A w/c ratio below 0.4 affects the binding properties, with the cement not obtaining maximum binding properties. It also affects the workability, where an increased amount of water increases the mobility of the concrete. It is, therefore, a compromise between the strength of the concrete and workability when w/c ratio is considered.

Luckily, it is possible to add admixtures to improve the properties and increase the workability of the concrete. Air entraining admixtures and superplasticizers are examples of admixtures affecting the concrete. This helps to increase the air void content, which is recommended to be between 4 – 6% to sustain frost. A lower value is acceptable for temperatures well above 0˚C. Superplasticizers can be added to increase the concrete's fluidity and workability, and it is reasonable to add if the w/c ratio is below 0.4. The superplasticizers will not affect the concrete strength [14].

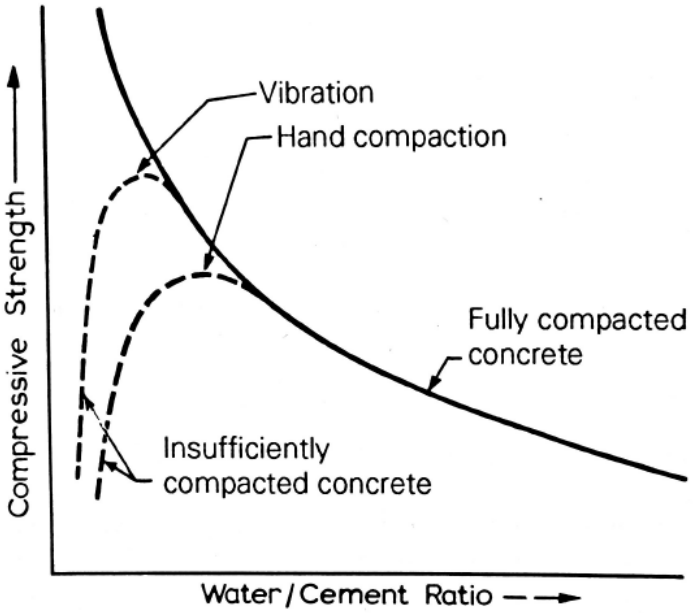

Figure 2: The relation between w/c ratio and the compressive strength of concrete [18].

2.1.2 Mechanical properties of concrete

The compressive strength of concrete increases with time, and the strength at age t depends on factors such as cement type, additional materials and temperature. The Eurocode 2: Design of Concrete Structures. Part 1-1: General rules and rules for buildings [19], shows that the characteristic compressive strength, f_{ck}, t days after casting is given as

$$\begin{cases} f_{ck}(t) = f_{cm}(t) - 8\ MPa & for\ 3 < t < 28\ days \\ f_{ck}(t) = f_{ck} & for\ t \geq 28\ days \end{cases}$$

where $f_{cm}(t)$ is defined as the mean value of concrete strength. This mean value develops with time by the relation

$$f_{cm}(t) = \beta_{cc}(t) f_{cm} \qquad (2.2)$$

where f_{cm} is the mean value of the unconfined concrete compressive strength after 28 days. β_{cc} is a coefficient depending on the age of the concrete:

$$\beta_{cc}(t) = \exp\left[s\left[1 - \left(\frac{28}{t}\right)^{\frac{1}{2}}\right]\right] \qquad (2.3)$$

where s is a coefficient depending on the type of cement, class R, N or S.

Eurocode 2 [19] gives the development of the tensile strength with time by

$$f_{ctm}(t) = \left(\beta_{cc}(t)\right)^{\alpha} f_{ctm} \qquad (2.4)$$

where α is a parameter depending on the concrete age

$$\begin{cases} \alpha = 1 & for\ t < 28\ days \\ \alpha = \frac{2}{3} & for\ t \geq 28\ days \end{cases}$$

2.1.3 Failure modes of concrete

Concrete is a brittle material that tends to fragment when subjected to dynamic loads such as ballistic impact. When a large amount of energy rapidly initiates, very high local stresses occur, and the material may fracture locally. Spalling and scabbing are the most common failure modes of concrete in ballistic impact cases. Spalling is defined as a failure in front of the target due to deformation and local inhomogeneity and anisotropy, while scabbing is defined as a failure in the rear side due to reflection of the compressive stress wave as tensile stresses [20]. A crater type of failure develops when pieces from concrete fall of from the structure as the reflected tensile waves exceed the capacity of concrete. This is a typical mechanism in materials strong in compression and weak in tension such as concrete.

The impact becomes harder as the loading rate increases and the failure mode of concrete plates will change from flexural bending to localized shear. This has been observed experimentally as the increased drop height of an impacting object gave more localized damage, and the failure mode was transferred from bending to local shear [21]. If the impact becomes harder, the duration decreases, and the time is suddenly too short for the stress wave propagation. As the amount of reinforcement increases, the failure is transferred from the center of the slabs to the supports, which is equivalent to from bending to shear [22].

Concrete goes through several failure modes when subjected to dynamic loading due to various states of stresses during the process. Severe hydrostatic compression takes place near the impacted area, and further away from the impact, the confinement stresses are reduced, and the material experiences compression with a moderate state of stress [23].

2.1.4 Fibers in concrete

Fibers are used in concrete to control cracks. They provide significant advantages compared to conventional concrete under static loads, and it also contributes to withstand extreme loads like explosion [24]. These fibers enhance many of the properties of high-strength concrete, including its tensile capacity, ductility, toughness and fragmentation resistance [25]. Others have observed that steel fibers in concrete produce a negligible effect on perforation resistance [26]. The use of them enhances the blast resistance and damage tolerance and improves control of displacements [25]. When they are used in ultra-high-performance concrete, the blast performance is improved by increasing the content of steel fibers from 2% to 4% [27]. Blast load experiments conducted by Tabatabaei et al. [28] show that the damage on reinforced concrete plates with compressive strength B52 decreases 75-89% when long carbon fibers are added into the concrete mix. Fibers also affect the water permeability by restricting the crack propagation [29], contributing to a higher safety for an SFTB surrounded by water. Zheng et al. [30] did some experiments with C60 fiber-reinforced concrete manufactured by vibratory mixing methods. The results show that the cube compressive strength and the flexural strength both increase with higher levels of fiber content.

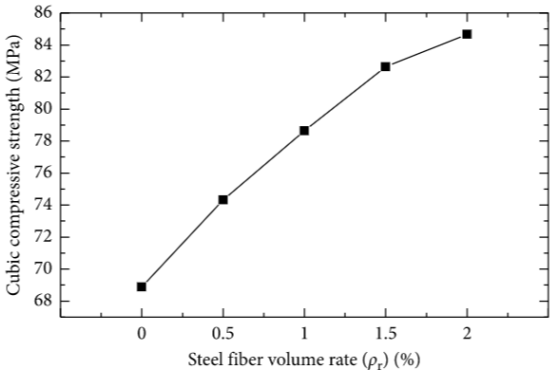

Figure 3: Relationship between cube compressive strength and steel fiber content [30].

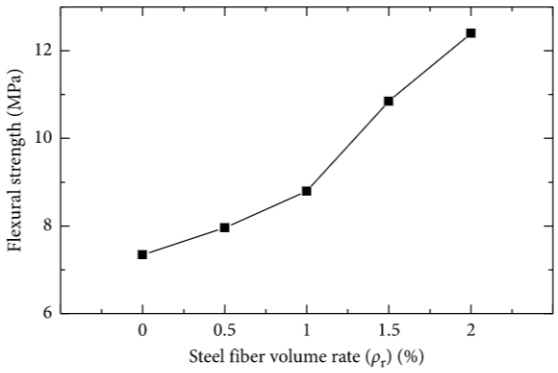

Figure 4: Relationship between flexural strength and steel fiber content [30].

2.1.5 Fire exposure in concrete

Concrete itself is a non-combustible material with excellent insulation properties. Fire may occur after a blast load, and the temperature will rise with time. Fire exposure will lead to spalling, which could impair the concrete by reducing its thickness and reducing the strength of reinforcement [31]. By adding PP-fibers to the concrete, the ability to withstand fire increases because it works as a passive fire protection. PP-fibers stand for

polypropylene fibers, where polypropylene is a thermoplastic polymer. Research has also shown that PP-fibers improve fire resilience for ultra-high-performance concrete [32-34].

The influence of high temperatures on the material properties of concrete, reinforcing steel as well as the stiffness and strength has been investigated in previous studies. Work done by Shu, J. et al. [35] studied if the reinforced concrete shells can carry the combination of fire and blast load if an accidental explosion occurs. The results showed that when the fire exposure time increased, the deflection was significantly increased, which indicated that the mechanical property of the concrete and reinforcement was degraded due to the high temperature. The compressive strength, tensile strength and stiffness of the reinforced concrete decreased by the fire exposure time.

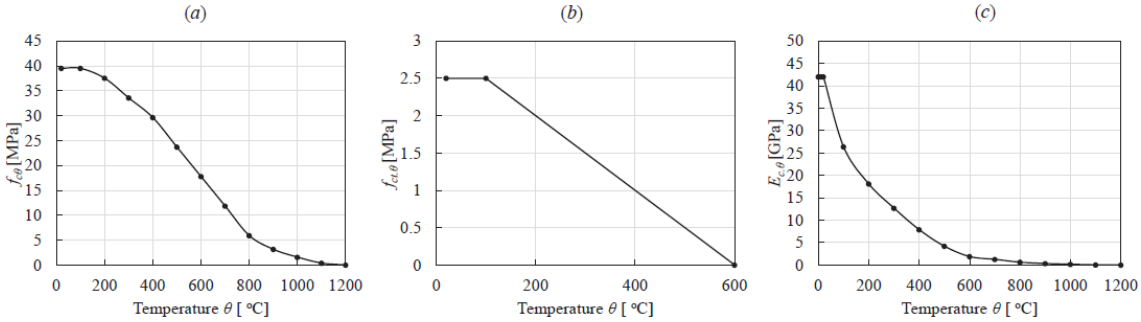

Figure 5: Material properties of concrete after exposed to fire: (a) Compressive strength, (b) Tensile strength, (c) Young's modulus [35].

2.2 Ballistic impact

The ballistic impact is a high-velocity impact by a small mass object. Ballistic is defined as the art of accelerating bodies using an engine, e.g., firearms and guns. The science of ballistics is divided into three main research areas: interior ballistics, which is the study of the motion and force acting on an object when it is still within the launcher, exterior ballistics, which is the study of the motion and forces acting on an object during free flight, and finally, the terminal ballistics, which describes the interaction between the object and the target during impact. In this thesis, the main focus is on terminal ballistics, which is the area of interest concerning fortification (structures used for additional strengthening) [20]. The word “impact” is defined as the collision between two or more solids, where the interaction between the bodies can be elastic, plastic or fluid, or any combination of these [20]. Ballistic threats are generally specified in terms of a projectile’s caliber, its impact kinetic energy, and the number of such impacts to be expected or tested [36].

The experiments are performed with a light-gas gun, which is a unique gun designed to generate very high velocities. It is used to research on impact phenomena, wherein this case, the impact is performed on concrete plates. How the concrete plates behave under ballistic impact, and what measures that can be applied to reinforce against these impacts is essential to know about, especially in protective structures. Penetration is defined as the entry of a projectile into any region of a target. The penetration may occur in different ways. According to Backman and Goldsmith [3], these definitions are suggested:

1) Perforation is if the projectile passes through the target with a final residual velocity.
2) Embedment is if the projectile is stopped within the target.
3) Ricochet or rebound is if the projectile is deflected from the target without being stopped.

Studies about ballistic impact by projectiles on concrete structures were carried out before or during World War II [37]. Analysis of reinforced concrete slabs hit by free-flying projectiles is challenging, and no fundamental theories can be applied to calculate with reasonable accuracy, only empirical formulas developed for the worst-case scenario of normal impact by nondeforming projectiles [38]. It seems that the use of reinforcement in concrete has a small effect on the perforation resistance [39].

The ballistic limit or limit velocity is defined as the average between the highest impact velocity not producing perforation, and the lowest impact velocity producing complete perforation. This velocity is of significant importance for the design of protective structures [20]. In addition to the ballistic limit velocity, the ballistic limit curve (impact versus residual velocity curve) is an essential measure in structural impact [20]. The curve gives the residual velocity as a function of the initial projectile velocity. It provides essential information to enable the design of an efficient passive safety structure to resist extreme loads. An explanation of passive safety structure is the effective resistance of a bullet penetrating armor to protect humans [40]. Another term is the ballistic limit line, i.e., the ballistic limit curve for a target with zero thickness. See Figure 6 for an illustration of the ballistic limit velocity, ballistic limit curve and ballistic limit line.

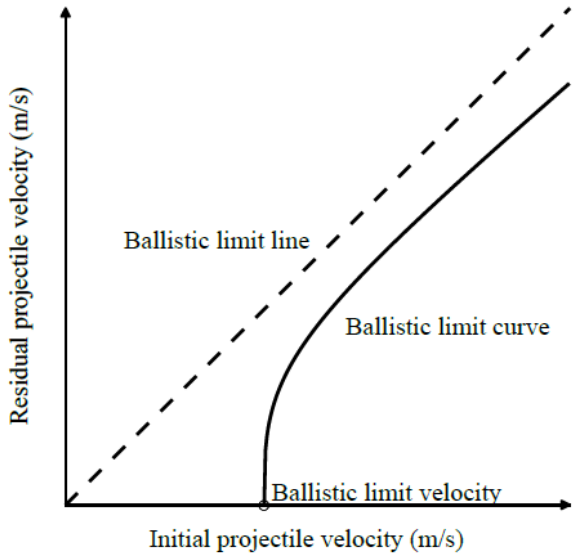

Figure 6: Definition of ballistic limit velocity, ballistic limit curve and ballistic limit line [20].

It appears that the penetration process is hardly affected by yaw angles of up to $3 - 5°$ based on experimental results reported by Goldsmith [41]. Larger angles may significantly reduce the penetration capacity of the projectile and need to be taken into consideration. It is, therefore, essential to measure projectile direction before and during the impact in order to see that the angle deviations are small enough to be neglected [20]. Complex coupling between projectile and target during impact makes most of the assessments assume that the projectile is fully rigid.

Impacted targets may fail in different ways. The actual mechanism will depend on material type and properties, projectile impact velocity, the shape of the projectile, trajectory, target support and relative dimensions of projectile and target. Projectiles with a sharp tip tend to have fragmentation as a perforating failure mode when a 50 mm thick concrete plate is the target. The fragmentation comes from high impact velocities with a large amount of energy deposited in a short time resulting in very high local stresses. The impact velocity is fundamental in impact mechanics, and the projectile velocity is so predominant that it overrides most other considerations [3]. The deformation in the target will be more localized with increasing velocity.

The most critical parameters for a complete description of an impact event seems to be [20]:

1. The trajectory and angle of incident of the projectile before impact.
2. Dynamic material properties of target and projectile.

3. Target thickness and boundary conditions.
4. Projectile diameter, mass and nose shape.
5. Mass ratio between target and projectile.

An experimental or numerical investigation of all parameters is a comprehensive work. It is, therefore, often simplified, and individual choices are taken regarding the significance of the different parameters. Many of the parameters are problem dependent and may be neglected in some penetration investigations [20].

When a projectile perforates a target, the impact itself generates a highly complex process of transforming kinetic energy into work. The kinetic energy is dissipated through many deformation mechanisms. The main ones are [20]:

1. Elastic deformation and vibration in both target and projectile, which may transfer energy to the supports and initiate plastic deformation throughout the plate.
2. Local plastic deformation of the plate, causing different types of failure or bulging.
3. Global plastic deformation of the plate, with considerable bending and membrane strains.
4. Projectile deformation and fracture.
5. Friction at the interfaces between the projectile and target.

It is important to emphasize that most of the experimental investigations reported in the open literature are carried out to validate existing theories and to develop the field further by pointing out potential improvements. Experiments are also essential to understand the underlying physics in the penetration cases.

The local and global deformation on the target is different from case to case. A general finding is that the global deformation changes rapidly as the target thickness increases, and hardly any global deformation is visible for the thickest targets. The global deformation depends both on the impact velocity and the target thickness. The localized shear zone will be very narrow in most penetration problems, giving a much higher temperature increase in that zone [20].

Increasing the density may produce a small increase in ballistic limit velocity, but increased compressive strength does not necessarily produce a comparable increase in the

ballistic resistance of concrete slabs impacted by projectiles. However, increased compressive strength decreases the penetration depth. Steel fibers have been observed to have a negligible effect on perforation resistance [37]. The significant difference between the outcoming results from target plates with and without steel fibers, is that the fragments from concrete with fibers seem to be generally bigger than fragments from concrete without fibers, where concrete without fibers has more pulverized debris [37]. Finite element method has several times been applied to ballistic impact problems, but perforation of concrete slabs is so complex that empirical equations in combination with physical tests are often used in design [42-45]. The limitation of empirical models is that they have a very strict and narrow range of validity. Extrapolation should not be used, and these models should be used with care and always in combination with the physical test when used to design [37].

2.2.1 Conservation laws

Conservation of mass, momentum and energy are substantial in physics and especially impact mechanics. The mass is constant within any system where the transformation of energy and matter is closed.

$$m = \int_V \rho dV = Constant \tag{2.5}$$

where ρ is the density of the material, and V is the volume of the material [20].

The conservation of momentum is expressed by the equation:

$$\sum_{i=1}^{n} m_i v_i = \int_V \rho dV = Constant \tag{2.6}$$

Conservation of momentum yields for a closed system of n masses m_i with respective velocities v_i, with no external forces performing the work itself.

Finally, the first law of thermodynamics gives [20]:

$$\Delta E_i = Q + W = \Delta K + \Delta U \tag{2.7}$$

ΔE_i is the change in internal energy, Q is the heat flow, W is the work, ΔK is the change in kinetic energy, ΔU is the change in potential energy.

In ballistic problems, there are no heat flow, i.e., Q = 0, and no change in potential energy, i.e., ΔU = 0. Conservation of energy leads to the work theorem for ballistic impacts [20]

$$W = \Delta K \tag{2.8}$$

2.2.2 Recht-Ipson model

The change of kinetic energy of the projectile can be estimated from work done on the concrete plate. Recht-Ipson model is an expression for the ballistic limit curve, that can be adjusted using curve fitting to find three parameters, v_{bl}, a and p. Recht and Ipson who developed this, considered normal impact of plates by blunt nose projectiles and thin plates, leading to plugging of the plates. The method can estimate the residual velocity of the projectile without the total amount of work used in the process, which is hard to identify. From work done in the inelastic impact with a plug entirely free from the plate, W_{free}, conservation of momentum can be used to estimate the velocity after impact. The shear work is done in the shear zone around the plug periphery (W_{shear}). Energy balance eliminates the shear work when assuming it is constant for initial velocities above ballistic limit velocity. Thus, it is estimated at the ballistic limit velocity, where $v_i = v_{bl}$ and the residual velocity $v_r = 0$.

$$W = W_{free} + W_{shear} = \Delta K = \frac{1}{2}\, m_p v_i^2 - \frac{1}{2}\left(m_p + m_{pl}\right) v_r^2 \tag{2.9}$$

where m_p and m_{pl} are masses of the projectile and the plug from the plate [20].
The rest of the parameters are defined as

$$W_{shear} = \Delta K - W_{free} = \frac{1}{2} m_p v_{bl}^2 - W_{free} \tag{2.10}$$

Resulting in

$$v_r = \left[\frac{m_p}{m_p + m_{pl}}\right] (v_i^2 - v_{bl}^2)^{\frac{1}{2}} \tag{2.11}$$

where v_i is the initial velocity and v_{bl} is the ballistic limit velocity.

a is defined as

$$a = \frac{m_p}{m_p + m_{pl}} \tag{2.12}$$

This model can be applied to pointed nose projectiles, where no plug is released from the perforation. Hence, m_p = 0 and a = 1.

$$v_r = \left(v_i^p - v_{bl}^p\right)^{\frac{1}{2}} \tag{2.13}$$

Lambert and Jonas generalized the Recht-Ipson model to arbitrary projectile nose shape as [20, 46]:

$$v_r = a\left(v_i^p - v_{bl}^p\right)^{\frac{1}{p}} \tag{2.14}$$

a, p and v_{bl} are material constants found from experiments. The projectile loses kinetic energy for the work to be done. Therefore, the ballistic limit curve must lie on the right side of the ballistic limit line, where $v_r = v_i$ and no energy is lost.

2.2.3 CEA-EDF perforation limit formula

The CEA-EDF [47] formula was developed in France in 1974, based on a series of drop weight impact and air gun experiments. The CEA-EDF formula is valid for projectile with incident velocities in the range of 20 – 200 m/s with a cube compressive strength between 18 – 46 MPa. The formula gives an estimate of the ballistic limit velocity on plain concrete subjected to hard missile impact from e.g., steel projectiles. The formula is expressed in this way:

$$V_p = 1.3\rho^{\frac{1}{6}} f_c^{\frac{1}{2}} \left(\frac{dH_0^2}{m}\right)^{\frac{2}{3}} \tag{2.15}$$

where V_p is the ballistic limit velocity in m/s, ρ is the density of concrete in kg/m^3, f_c is the unconfined compressive strength of concrete in N/m^2, d is the diameter of the projectile in m, H_0 is the thickness of the target in m, and m is the mass of the projectile in kg.

The CEA-EDF perforation limit formula is an empirical formula based on experiments. As mentioned earlier, such formulas have limitations with a very strict and narrow range of validity.

2.2.4 Nose shape of projectiles

The effect of an impact is dependent of the nose shape of a projectile. The shape of it determines how extensive the damage of the target will be. Below, different shapes are described based on performed tests.

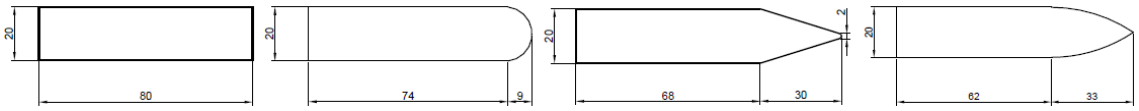

Figure 7: Geometry of blunt, hemispherical, conical and ogival nosed projectiles [20].

A graph describing the relation between initial projectile velocity and residual projectile velocity for the different nose shapes is shown in Figure 8.

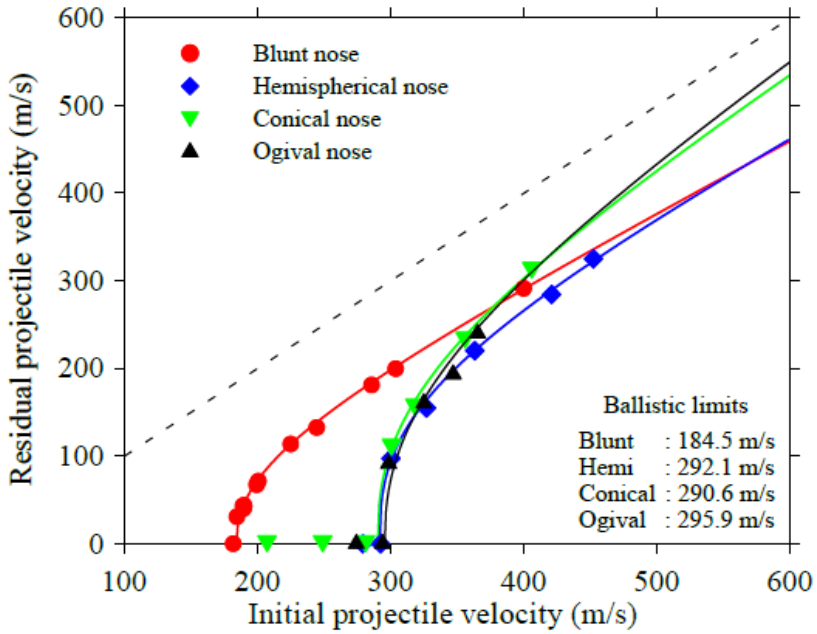

Figure 8: Ballistic limit curves for blunt, hemispherical, conical and ogival projectiles [20].

The blunt projectile has a lower initial projectile velocity, which is logical based on its geometry. The blunt projectile has an outer area at the tip larger than the others, which makes the drag force higher. Thus, it decreases its initial velocity before it hits the plate. The ogival projectile has the highest initial velocity, with the other sharp ended projectiles following along. The difference in slope between the various initial-residual velocity curves comes from the difference in energy absorption during impact, where the blunt projectile loses more energy compared to the other nose shapes. The blunt shape deforms almost exponentially with impact velocity in the actual velocity regime, while pointed projectiles hardly get deformed during impact [20].

Figure 9: Different kind of projectiles used in experiments at NTNU [photo taken by author].

2.2.5 Ballistic impact of concrete plates

Ballistic impact of concrete plates is a complex topic, and it is essential to recognize that penetration and perforation mechanics in concrete is relatively more complex than in metals due to its complex material behavior and distinct characteristics under tension and compression [47]. Even though a lot of empirical and analytical models have been proposed for estimating projectile penetration in concrete targets [4, 48-51], these models are based on the appropriate experimental validation.

Many studies have been conducted on ballistic performances of concrete targets subjected to steel projectile impact. Different conditions have been tested, e.g., plain concrete, reinforced concrete and prestressed concrete. Most of the concrete is reinforced in the real world. The tensile strength improves with the combination of steel as a material, and as expected, it gives a higher resistance against ballistic performances. Rajput et al. [52] conducted an experimental and numerical test with 0.5 and 1 kg ogival nosed hardened steel projectiles, where the conclusion was that the ballistic limit of reinforced concrete was found to have increased by 14% compared to plain concrete. During the experiments, the targets of both plain and reinforced concrete were found to experience complete perforation at high velocities and underwent local damage at the front as well as the rear surface. The presence of reinforcement prevented scabbing of the concrete material. A numerical study with the Holmquist-Johnson-Cook material model was performed on the same case resulting in a lower deviation between actual and simulated ballistic limit for reinforced concrete compared to plain concrete. This study tells something about the impact reinforcement in concrete has on numerical simulations to predict accurate results.

The failure of plain concrete occurred through sudden radial cracks coming from the center of the target, resulting in splitting the concrete. The numerical simulation could not predict the radial cracking and splitting in concrete.

The penetration depth on grout and concrete targets by steel projectiles was experimented by Forrestal et al. [53]. The experiment showed that the penetration depth increased in the concrete (from 200 to 1000 mm) with an increase in the striking velocity (350 – 1200 m/s) until the nose erosion became excessive. Mu and Zhang [54] did experiments with steel ogival projectiles struck against concrete targets at impact velocities ranging from approximately 500 m/s to 1500 m/s. The observation was that impact velocity larger than a critical value made the depth of penetration decrease dramatically. The projectile nose changed from ogive to hemisphere indicating a transition from rigid penetration to deformable or erosive penetration. It is, therefore, essential to consider the effect of abrasion of the nose shape of the projectile during accurate analysis.

Spalling and scabbing are two terms that are used in studies of concrete perforation. Spalling is the term used for the damage that occurs on the front side of the plate where the projectile first enters. Scabbing is the term used for the damage that occurs on the rear side of the plate where the projectile leaves.

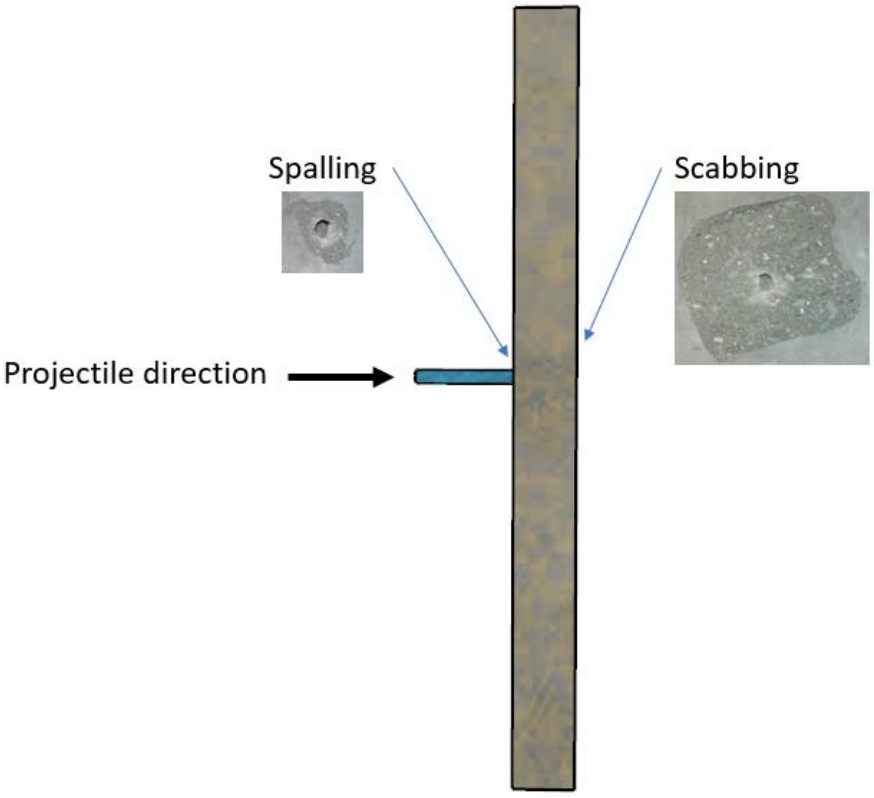

Figure 10: Spalling and scabbing after perforation.

Studies by Rajput et al. [52] showed that for a given concrete type, the diameter of the rear surface crater decreased with the increase in incidence velocity. It can be imagined as a situation where velocity makes the concrete unaware that perforation is occurring, and therefore the surface crater gets less affected. It is likely to believe that the scabbing of the material increases with the decrease in striking velocities until the attainment of the ballistic limit. The reduction in the size of the crater with increasing velocity was more significant in reinforced concrete compared to plain concrete. In both plain and reinforced concrete, the targets experienced more scabbing against a heavier projectile compared to a lighter projectile. That makes sense in the way that more mass leads to more destruction. The resistance of the concrete targets was therefore found higher against 0.5 kg projectile in comparison to the 1 kg projectile, something that requires the lighter projectile to have a higher velocity in order to perforate the concrete plate. The reinforced concrete targets offered a higher ballistic limit since the reinforcement grid provided partial confinement to the concrete plates; hence, pressure wave propagation was very slow in the reinforced concrete target.

Rajput et al. [47] also studied the ballistic performance of plain, reinforced and prestressed concrete targets of unconfined compressive strength 48 MPa. The experiments were done with target thicknesses 60, 80 and 100 mm. They were subjected to normal impact by 1 kg ogive nosed hardened steel projectiles of diameter 19 mm and length 450 mm. Varying incident velocities from 65 to 220 m/s were used. The reinforcement in the concrete was found to be effective in minimizing the spalling and scabbing of material. The prestressing stimulated the globalization effect in the deformation process and improved the ballistic performance. The ballistic limits of the reinforced concrete targets were higher compared to the plain concrete targets. On the other hand, the ballistic limits of prestressed concrete targets were found to be higher than the reinforced concrete targets.

Increasing projectile velocity produces cracking of the concrete on the rear side followed by scabbing. And once the scabbing starts, the depth of penetration increases fast with increasing velocity, which leads to perforation of the target when the penetration hole extends through the scabbing crater [4]. The scabbing and perforation occur together in plain concrete since there is no reinforcement to restrain the shear cone [49]. A common way to improve the ballistic resistance of concrete is to add a steel cladding to the front

and rear surface to avoid scabbing and/or spalling of material. A comparison between reinforced concrete with and without clad showed the benefits of steel cladding, with a significant increase in the impact resistance with rear face clad panels compared to front face clad panels [55]. Another essential technique to improve the ballistic performance is by avoiding premature tension failure by applying initial prestressing force. The prestressing in the concrete is highly effective in improving the load-carrying capacity and reducing sections and crack width in structural elements [47].

Dancygier and Yankelevsky [56] found that 40 – 60 mm thick high strength (104 MPa) concrete targets gave higher ballistic resistance than normal strength (34 MPa) concrete targets. The concrete penetration could be divided into three different modes depending on the initial impact velocities: penetration by a quasi-rigid penetrator, penetration by a deformable penetrator and penetration by an erosive penetrator [57]. Quasi-rigid penetration is, for example, when an ogival projectile penetrates a concrete target with mass loss due to abrasion. Wen et al. [58] proposed a formula for projectile penetrating concrete target by a dimensional analysis which can be expressed as

$$\frac{\Delta m}{m} = p\left(Moh \cdot \frac{\rho_t}{2Y_p} V_o^2\right)^q \qquad (2.16)$$

where Δm is the mass loss because of abrasion, m_0 is the original projectile mass, V_o is the impact velocity, Y_p is the dynamic projectile strength, ρ_t is the target density, Moh is the Mohr hardness of concrete target aggregate, p and q are dimensionless empirical constants and can be taken as p = 0.0162 and q = 0.805 [58]. Experiments by Forrestal et al. [53] led to observations of deforming projectiles, where ogival-nosed projectiles changed shape from ogival to blunt, or sometimes hemispherical when the impact velocity was high enough.

2.3 Finite Element Method (FEM)

The finite element method is used as a numerical problem-solving methodology in many engineering fields for numerous applications. The applications are wide such as fluid flow, structural analysis, heat transfer, collisions and blast loading. The method attempts to approximate the values of the unknowns, which is to be solved. The method subdivides the main problem into smaller sub-issues that are easier to solve. The sub-issues are called

finite elements and require implicit and/or explicit analysis. The method is used to assess the design for tension, weak spots and other critical information before implementing to the original design.

There are two main types of finite element methods, which are the implicit and explicit finite element methods. The implicit method is used when events occur on a moderate level, and the strain rates are minimal. When the growth of stress as a function of strain is produced, these can be analyzed with implicit methods. Many of the engineering problems around the world get covered by the implicit method. In an implicit method, one can consider a static equilibrium:

$$Sum\ of\ all\ forces = 0 \tag{2.17}$$

The explicit method is used when the strain rates/velocity is above 10 units/second or 10 m/s respectively. Examples on scenarios applicable to the explicit method are ballistic impact and blast loading. The material models need to account for the strain rate along with the accounting for the variation of stress with strain, where the strain rates have a significant effect on the results. The explicit method is used in events where there is a dynamic equilibrium or otherwise:

$$Sum\ of\ all\ forces = mass \times acceleration \tag{2.18}$$

2.3.1 Explicit Finite Element Method

According to work by O.S. Hopperstad and T. Børvik at NTNU [59], the explicit finite element analysis is well suited to solve transient dynamic problems, e.g., explosions and structural impacts. This method is also used in highly nonlinear quasi-static problems, such as plastic forming. In both these problems, a short time-step is needed because of the high rates of strain. Explicit FEM is suitable since it does not need as many iterations in each time-step as in the implicit integration method. It is essential to notice that the explicit FEM is not stable for every time step, and therefore it must be checked to make sure that the results are adequate.

2.4 Material models

Relevant material models that describe the behavior of concrete exposed to dynamic loads are presented. The models are mathematical representations of the expected behavior of concrete. The material models are applicable to numerical simulation programs and make sure that the simulation considers the material properties during analysis. The original Holmquist-Johnson-Cook, the modified Holmquist-Johnson-Cook model and the JH-2 model are the material models presented.

2.4.1 Original Holmquist-Johnson-Cook material model

The material properties specified by the material law determines the shape of the yield surface. To model the material characteristics in concrete, the original Holmquist-Johnson-Cook (HJC) material model is an adequate option. The theory in the original HJC model is found in Holmquist et al. [43] and M. Polanco et al. [42]. In this model, the yield function is given by the normalized equivalent stress, determined by the constitutive relation

$$\sigma_{eq}^{*} = \frac{\sigma_{eq}}{f_c} = \left[A(1-D) + BP^{*N}\right]\left[1 + C\ln\dot{\varepsilon}_{eq}^{*}\right] \leq S_{max} \quad , \quad P^{*} \geq 0 \qquad (2.19)$$

where σ_{eq} is the equivalent stress, f_c is the quasi-static uni-axial compressive strength, A is the cohesion parameter, B is the pressure hardening coefficient, N is the pressure hardening exponent, C is the strain-rate sensitivity coefficient and $\dot{\varepsilon}_{eq}^{*}$ is the normalized strain rate. The normalized pressure is defined as $P^{*} = P/f_c$. When the normalized pressure reaches negative values, $P^{*} < 0$, the normalized hydrostatic tension $T^{*} = T/f_c$ is used in the expression of σ_{eq}^{*} instead. Here, T is the maximal hydrostatic tension the material can resist. The normalized equivalent stress from the HJC model has a point of discontinuity at $P^{*} = 0$. S_{max} is the normalized maximum developed strength. Further, material degradation is considered by the damage variable D, in which a high percentage of this variable results in reduced cohesive strength. The scalar damage formulation is a part of the HJC model and is given in [42] by the expression

$$\Delta D = \frac{\Delta\varepsilon_{eq}^{p} + \Delta\mu_{eq}^{p}}{\varepsilon_{p}^{f} + \mu_{p}^{f}} \qquad (2.20)$$

where $\Delta\varepsilon_{eq}^{p}$ is the equivalent plastic strain increment and caused by plastic shear deformation. Plastic crushing of air voids in concrete is represented by the equivalent plastic volumetric strain increment $\Delta\mu_{eq}^{p}$. The plastic strain to fracture $\varepsilon_p^f + \mu_p^f$ is a function expressed in [42] as

$$\varepsilon_p^f + \mu_p^f = \alpha(P^* + T^*)^\beta \geq \left(\varepsilon_p^f\right)_{MIN} \qquad (2.21)$$

in which α and β are material constants. To prevent fracture from low magnitude tensile waves, a finite amount of plastic strain can crack up the material. Therefore, the lower limit $\left(\varepsilon_p^f\right)_{MIN}$, i.e., the minimum strain at fracture, is introduced as a threshold value in this expression.

The original HJC model describes many essential aspects of the concrete behavior, such as pressure- and rate dependency, damage cracking and compaction. The model is not, however, entirely comprehensive to describe all the essential concrete mechanisms, and the description is also discontinuous. Polanco-Loria et al. [42] made some modifications to the original Holmquist-Johnson-Cook material model to improve the prediction of the ballistic limit for the concrete slab. This was done by mainly focusing on the compressive behavior and strain-rate effect of concrete. Since the HJC material model does not describe the pressure-shear strength difference in tensile and compressive meridians, this model was discontinuous. By introducing a third stress invariant, i.e., the Lode parameter, the original HJC gets a continuity in its description of the pressure-shear behavior. This makes the HJC material model relevant both for shear strength differences in tensile and compressive meridians. Another adjustment applied to the model is the change in strain rate sensitivity, which is changed so that the strain rate enhancement factor goes to unity for zero strain rate. The third proposed modification of HJC is to apply three damage variables to describe tensile cracking, shear cracking and pore compaction mechanisms.

2.4.2 Modified Holmquist-Johnson-Cook material model

According to M. Polanco et al. [42] the material characteristics in concrete could also be modeled through the Modified Holmquist-Johnson-Cook (MHJC) material model. This is a modification of the original HJC model. The purpose of the modified HJC model is to avoid the discontinuity of the normalized equivalent stress and circumvent the cohesion parameter A. To express the yield function, the normalized equivalent stress is given as

$$\sigma_{eq}^{*} = \frac{\sigma_{eq}}{f_c} = \begin{cases} B[P^* + T^*(1-D)]^N F(\dot{\varepsilon}_{eq}^{*}) R(\theta, e) \leq S_{max} \\ for\ P^* \geq -T^*(1-D) \\ 0\ for\ P^* < -T^*(1-D) \end{cases} \qquad (2.22)$$

in which B, P* T*, N and S_{max} are corresponding to the parameters in the HJC model, while the damage, D, is defined between 0 and 1. Tests should be done to set valid values to the parameters, which are related to the stress-strain curve to failure both for uniaxial and triaxial compression. $\dot{\varepsilon}_{eq}^{*} = \dot{\varepsilon}_{eq}/\dot{\varepsilon}_0$ is the dimensionless strain rate, where $\dot{\varepsilon}_{eq} = \sqrt{\frac{2}{3} D'_{ij} D'_{ji}}$ is the normalized strain rate and the reference strain rate is set to $\dot{\varepsilon}_0 = 1$. D'_{ij} is the deviatoric part of the rate-of-deformation tensor. To describe the strain rate influence, the function $F(\dot{\varepsilon}_{eq}^{*})$ *is* introduced. This strain rate influence is given in [42] as the function

$$F(\dot{\varepsilon}_{eq}^{*}) = \left[1 + \dot{\varepsilon}_{eq}^{*}\right]^{C} \qquad (2.23)$$

where the strain rate sensitivity parameter C describes the non-linear character of the rate effect.

The reduction of shear strength on the compressive meridian is considered by the function $R(\theta, e)$, given in [42] by

$$R(\theta, e) = \frac{2(1-e^2)cos\theta + (2e-1)[4(1-e^2)cos\theta^2 + 5e^2 - 4e]^{1/2}}{4(1-e^2)cos\theta^2 + (1-2e)^2} \qquad (2.24)$$

where e is the shape factor describing the out-of-roundness of the yield surface in the deviatoric plane. This out-of-roundness parameter represents the portion of strength on the tensile meridian compared to the compressive meridian. To obtain a function with convexity and smoothness, e must be set as a value between 0.5 and 1.0. When the value of $e = 0.5$, the function is forming a triangle in the deviatoric plane. In the same way, if $e = 1.0$, the result is a circular shape in the deviatoric plane. The parameter θ is called the deviatoric polar angle and given in [42] as

$$\theta = \frac{1}{3} cos^{-1}\left(\frac{27|S_{ij}|}{2\sigma_{eq}^3} \right) \qquad \text{for } 0° < \theta < 60° \qquad (2.25)$$

In this definition, $|S_{ij}|$ is the determinant of the deviatoric stress tensor S_{ij}, where the deviatoric polar angle $\theta = 0°$ corresponds to a generalized state of tensile stress. At the

upper angle boundary, $\theta = 60°$, the generalized state of compressive stress is found. According to D. Morin et al. [60], the coupling between the deviatoric polar angle, θ, and a Lode parameter, L, is expressed in [42] as

$$L = \sqrt{3} tan\left(\theta - \frac{\pi}{6}\right) \tag{2.26}$$

Further, the lecture notes by O.S. Hopperstad and T. Børvik [59] defines the lode parameter as

$$L \equiv \frac{2\sigma_{II} - \sigma_I - \sigma_{III}}{\sigma_I - \sigma_{III}} = \frac{3\sigma'_{III}}{\sigma'_{II} - \sigma'_{III}} \tag{2.27}$$

where $\sigma_I \geq \sigma_{II} \geq \sigma_{III}$ is the ordered principal stress. The ascending order of the principal deviatoric stress is $\sigma'_I \geq \sigma'_{II} \geq \sigma'_{III}$, given by $\sigma'_i = \sigma_i - \sigma_H$, with $i = I, II, III$. Since the Lode parameter depends on the principal stresses, which are invariants, the Lode parameter is an invariant as well. According to the definition of the Lode parameter, $L = +1$ is equivalent to $\theta = 60°$ and value of the Lode parameter $L = -1$ is equivalent to $\theta = 0°$. These two Lode parameters describe states of generalized compression, $\sigma_I = \sigma_{II} \geq \sigma_{III}$, and generalized tension, $\sigma_I \geq \sigma_{II} = \sigma_{III}$. To state the generalized shear, the Lode parameter is set to zero. At this value of the Lode parameter, the shear stress dependency is represented, i.e., the differentiation of the tensile and compressive meridians [59].

To define the relation between pressure, P, and volumetric strain, μ, MHJC separates the material behavior into three regions in compression. The first region has a linear elastic behavior and limited by P_{crush} and μ_{crush}. In the second region, after the pressure has reached P_{crush} and the volumetric strain is at μ_{crush}, the compression causes production of plastic volumetric strains and crushing of concrete. When the air voids are entirely compressed, the third region of compression is reached, starting at (P_{lock}, μ_{lock}). To model the third region, the concrete slab is completely elastic, without tensile capacity.

M. Polanco et al. [42] explains that three damage mechanisms are always acting in brittle materials. These mechanisms are tensile cracking, shear cracking and pore compaction. In the original HJC model, these damage mechanisms are merged into one damage parameter, while MHJC separates them. The damage parameters in MHJC are D_T, D_S and D_C, representing tensile cracking, shear and compaction damage, respectively. The damage that occurs from tensile cracking is ignored because of the contribution from the

steel reinforcement. Thus, the damage parameter D_T is excluded in the calculation of the total damage effect. The total damage effect is given by

$$(1 - D) = \sqrt{(1 - D_S)(1 - D_C)} \tag{2.28}$$

In this description, the evolution of the shear damage variable D_S is expressed in [42] as

$$\Delta D_S = \frac{\Delta \varepsilon_{eq}^p}{\varepsilon_p^f} \tag{2.29}$$

where $\Delta \varepsilon_{eq}^p$ is the equivalent plastic strain increment, caused by plastic shear deformation. The denominator in the equation is the plastic strain to fracture, ε_p^f, which is taken from the original HJC model. Further, finding the internal compaction damage variable, D_C, is found in [42] through the expression

$$\Delta D_C = \frac{\Delta \mu^p}{\mu_{lock}} \tag{2.30}$$

where $\Delta \mu^p$ is the incremental plastic volumetric strain. The plastic volumetric strain of the fully compacted granular material, μ_{lock}, is the upper limit for the plastic volumetric strain, formulated in [42] as

$$\mu_{lock} = \rho_{grain} / \rho_0 - 1 \tag{2.31}$$

where ρ_{grain} is the grain density and ρ_0 is the initial density.

The modified HJC model includes the influence of the third deviatoric stress invariant and introduces three damage variables describing the tensile cracking, shear cracking and pore compaction mechanisms. This material model is suitable for large-scale computations of concrete plates impacted by projectiles [61].

2.4.3 JH-2 model

JH-2 is the second version of the Johnson-Holmquist (JH-1) ceramic model [62] used to simulate the impact behavior of brittle materials such as dilatation, pressure-strength dependence, strain-rate effect by damage [63]. JH-2 is an improved computational constitutive model for brittle materials, which is possible to simulate with the ABAQUS software and works well for computations in both Lagrangian and Eulerian codes. The model is applicable for brittle materials as concrete exposed to large strains, high strain rates and high pressures. However, the computational framework for the analysis of these

materials is less developed than their metallic counterparts [64]. The equivalent strength is dependent on intact strength, fractured strength, strain, strain rate, pressure and damage. The pressure considers bulking as an effect, which comes through the transfer of internal energy from decreased shear and deviator stresses to potential internal energy related to increased hydrostatic pressure [63].

The strength in the model is defined as the equivalent stress as follows:

$$\sigma^* = \sigma_i^* - D(\sigma_i^* - \sigma_f^*) \tag{2.32}$$

σ_i^* is the normalized intact equivalent stress, D is the damage variable and σ_f^* is the normalized fractured equivalent stress.

It is essential to notice that the intact material is represented by the damage value D = 0, and the fully damaged material is represented by the damage value D = 1. The equation of the strength in undamaged and fully damaged material states can be described as a function of pressure and strain rate:

$$\sigma_i^* = A(P^* + T^*)^N(1 + Cln\varepsilon^*) \leq \sigma_i^{max} \tag{2.33}$$

and

$$\sigma_f^* = B(P^*)^M(1 + Cln\varepsilon^*) \leq \sigma_f^{max} \tag{2.34}$$

where the material parameters are A, B, C, M and N. The strength limits are defined as σ_i^{max} and σ_f^{max}, and the normalized pressure is defined as

$$P^* = \frac{P}{P_{HEL}} \tag{2.35}$$

where P is the actual pressure and P_{HEL} is the pressure at the Hugoniot Elastic Limit. The normalized maximum tensile hydrostatic pressure could also be written as

$$T^* = \frac{T}{T_{HEL}} \tag{2.36}$$

where T is the maximum tensile pressure that the material supports. The JH-2 model uses damage accumulation similar to the JH-1 model [62] and assumes the damage to increase along with the plastic strain as

$$D = \sum \frac{\Delta\bar{\varepsilon}^{pl}}{\bar{\varepsilon}_f^{pl}(p)} \tag{2.37}$$

where

$$\bar{\varepsilon}^{pl} = D_1(P^* + T^*)^{D_2} \; ; \; \bar{\varepsilon}^{pl}_{f,min} \leq \bar{\varepsilon}^{pl} \leq \bar{\varepsilon}^{pl}_{f,max} \tag{2.38}$$

$\Delta\bar{\varepsilon}^{pl}$ is the increment of the equivalent plastic strain, and $\bar{\varepsilon}^{pl}_f(p)$ is the equivalent plastic strain to fracture under a constant pressure, p. D_1 and D_2 represent material constants. $\bar{\varepsilon}^{pl}_{f,min}$ and $\bar{\varepsilon}^{pl}_{f,max}$ are introduced for the limitation of minimum and maximum values of the fracture strain. The pressure-volume relationship for brittle materials is defined as

$$P = \begin{cases} K_1\mu + K_2\mu^2 + K_3\mu^3 & if\ \mu \geq 0\ (compression) \\ K_1\mu & if\ \mu < 0\ (tension) \end{cases} \tag{2.39}$$

where K_1, K_2, K_3 are material constants, and $\mu = \rho/\rho_0 - 1$ with ρ as the current density, and ρ_0 as the reference density. An additional pressure increment ΔP is included when the material fails. This can be expressed as

$$P = K_1\mu + K_2\mu^2 + K_3\mu^3 + \Delta P \tag{2.40}$$

The determination of the pressure increment is done by energy consideration. The deviatoric elastic energy ΔU decreases due to the decrease of strength when the material is damaged. Figure 11 illustrates the relationship of pressure-volumetric strain based on the JH-2 model [65].

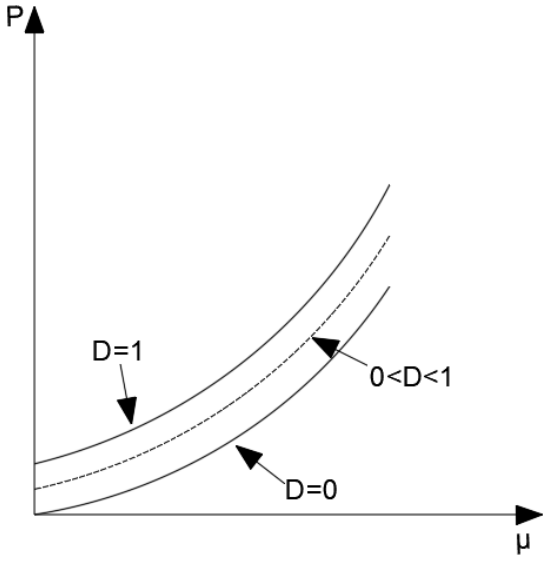

Figure 11: Pressure-volumetric strain relationship in the JH-2 model.

The elastic energy decreases and converts into potential energy by the increase of the pressure increment ΔP:

$$\Delta P_{t+\Delta t} = -K_1\mu_{t+\Delta t} + \sqrt{((K_1\mu_{t+\Delta t} + \Delta P_t)^2 + 2\beta K_1 \Delta U} \qquad (2.41)$$

where β is the fraction of the elastic energy increase, which is converted to potential energy ($0 \leq \beta \leq 1$).

The JH-2 material model is more developed compared to the original Holmquist-Johnson model for brittle materials (JH-1). JH-1 does not allow for gradual softening. Another weakness with JH-1 is that the results are very sensitive to changes in the constants used in the model, with no straightforward process to determine accurate constants. The last weakness with JH-1 is the jump conditions between fractured material (damage = D = 1.0) and intact material (D < 1.0), which causes problems for Eulerian codes, where the material tends to heal itself after a fracture has occurred [63].

The JH-2 material model begins to soften when the damage starts to accumulate (D > 0), and this allows for gradual softening under increasing plastic strain. In the JH-1 material model, the softening occurs rapidly when D = 1.0, and not before. Another strength with the JH-2 model is that the strength and damage are analytical functions of the pressure, which allows for variation of the constants in a more systematic manner. In comparison, the JH-1 uses multiple linear segments [63].

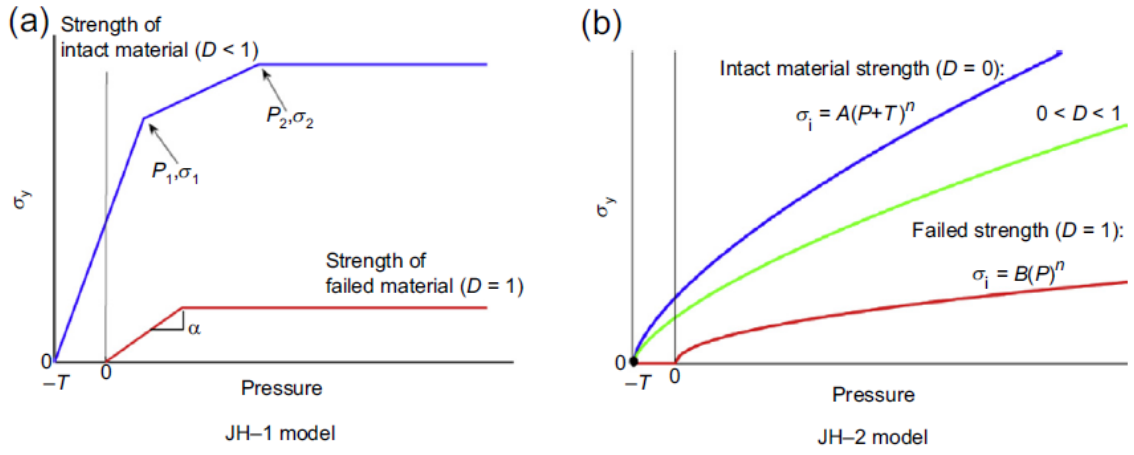

Figure 12: Comparison between JH-1 and JH-2 [64].

2.5 Numerical simulations of ballistic impact problems

Numerical simulations have rapidly evolved to understand complex dynamic events, with the benefit of reduced cost, increased speed and attention in detail. The numerical model is built up with material response calculated in an iterative, stepwise way, where

incremental elements of strain lead to changes in stress through a material constitutive equation. The modeler has the opportunity to choose between 2D or 3D finite element method, and linear or nonlinear material behavior [64].

Review of existing numerical studies is done to understand the numerical modeling of the ballistic impact. The setup of simulations is essential before executing a simulation. Further, the function of parameters is explored to get a better understanding. A rapid development in the industry when it comes to computer technologies makes the numerical simulation an efficient and economical alternative to experiment as a research method for ballistic impact on concrete [61]. When the numerical simulations can render the results from the experiments, it is possible to expand the simulated model and predict the outcome of a whole structure [2].

2.5.1 Setup of the numerical simulations

The setup of numerical simulation is essential to obtain sensible results from the simulations that renders the experimental results. If accuracy is important, then various material tests, including quasi-static uniaxial tensile tests, uniaxial compressive tests, hydrostatic compressive tests, and triaxial compressive tests with various confinement pressure have to be done to get good parameter values for the simulations [61]. Empirical values and equations could be used for some parameters if corresponding material test data are unavailable [66].

An example of this is found in research by Polanco-Loria et al. [42]. Here, the FE analyses were performed with the LS-DYNA software by using 2D axisymmetric elements with a reduced integration scheme with hourglass control, as illustrated in Figure 13. The MHJC material model is used to describe the behavior of concrete in this numerical simulation. The mesh had 100 elements over the target thickness. The mesh size, mesh bias, friction effects and erosion strain parameters are relevant in this context. The steel reinforcement had a negligible impact on the perforation resistance of the concrete specimen and was therefore excluded from the simulation. To model the steel projectile, a Von Mises material model was applied together with a linear isotropic hardening model.

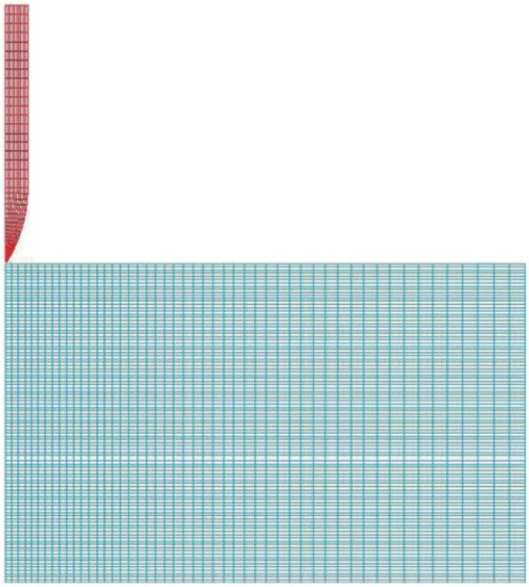

Figure 13: Illustration of the axisymmetric elements [42].

2.5.2 Results from existing numerical simulations

The feature of predicting the results from experiments is essential for numerical simulations. In this section, the attempt to render a ballistic impact test is described through a literature review.

Different authors have written about the rendering of experimental results, e.g., Børvik et al. [67], Dey et al. [68] and Holmen et al. [69], where high-strength steel plates perforated by a steel projectile were inspected. An important point from these papers was that a FE analysis software could predict the results from the experiments.

The experimental study of the ballistic impact conducted by Hanchak et al. [39] constitutes the reference model for the MHJC model. The reinforced concrete plates used in this test had a dimension of 610x610x178 mm with concrete quality of C48 and C140. An ogival projectile with a mass of 0.5 kg, a diameter of 25.4 mm, and a total length of 143.7 mm represented a fragment in this test and was fired at the specimen. The resulting values were used to draw initial versus residual velocity curves for the two concrete qualities, and further to deduce the ballistic limits. They concluded that the ballistic limit velocity only increased by 20% when the compressive strength of the concrete increased with a factor of three.

The research paper written by Polanco-Loria et al. [42] describes the process of establishing a numerical simulation. Here they wanted to see if the MHJC model could

render the same results as the experiments done by Hanchak et al. [39]. The input parameters in this model are presented in Table 1 for C48 and Table 2 for C140.

Table 1: Material parameters for C48 concrete [42]. The definition of these parameters is described in section 2.4.2.

ρ_0 (kg / m^3) 2440	E (MPa) $11700(f_c)^{0.3}$	ν 0.2	B 1.4	N 0.65	C 0.04	S_{max} 7
f_c *(MPa)* 48	f_t *(MPa)* 4	$\dot{\varepsilon}_0$ *(s^{-1})* 10^{-5}	α 0.04	β 1.0	$(\varepsilon_p^f)_{MIN}$ 0.01	
P_{crush} *(MPa)* 16	μ_{crush} $f_c\,(1 - 2\nu) / E$	P_{lock} *(MPa)* 800	μ_{lock} 0.1	K_1 (MPa) 8500	K_2 (MPa) -17100	K_3 (MPa) 20800

Table 2: Material parameters for C140 concrete [42]. The definition of these parameters is described in section 2.4.2.

ρ_0 (kg / m^3) 2520	E (MPa) $11700(f_c)^{0.3}$	ν 0.2	B 1.30	N 0.45	C 0.025	S_{max} 7
f_c *(MPa)* 140	f_t *(MPa)* 5	$\dot{\varepsilon}_0$ *(s^{-1})* 10^{-5}	α 0.04	β 1.0	$(\varepsilon_p^f)_{MIN}$ 0.004	
P_{crush} *(MPa)* 46	μ_{crush} $f_c\,(1 - 2\nu) / E$	P_{lock} *(MPa)* 800	μ_{lock} 0.04	K_1 (MPa) 8500	K_2 (MPa) -17100	K_3 (MPa) 20800

The results from the numerical predictions of the residual velocity are similar to the results from the experiments for both concrete qualities, as illustrated in Figure 14.

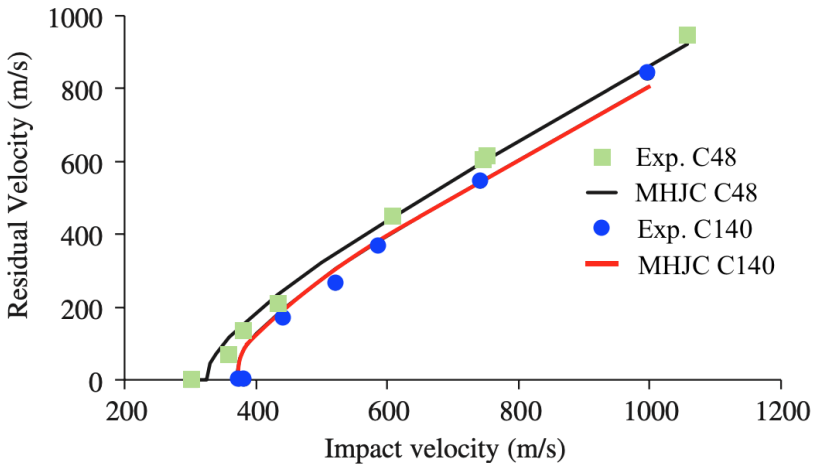

Figure 14: Ballistic limit predictions using the MHJC for C48 and C140 concrete qualities [42].

The research paper by Polanco-Loria et al. [42] concludes that both the original and modified HJC model can render the results from the ballistic impact test by Hanchak et al. [39]. Further, it is expected that these models give substantial differences in the results when the projectiles penetrate either thin slabs or massive blocks. Therefore, enhancements must be applied in the original HJC model to avoid the discontinuity at $P^* = 0$ and to obtain more similar results.

2.5.3 Parameter study with numerical simulations

The chosen values of parameters in numerical simulations have a significant impact on the results. Therefore, these parameter values must be chosen wisely to render the results from the experiments. The friction parameter is selected to show how the results change due to a change in the value of this variable.

Element deletion is an approximate approach when it comes to simulating cracks as a simple technique. Loss of mass, momentum and energy due to element deletion may cause errors in, for example, residual velocity. The normal practice is to apply erosion algorithm by setting a value for the equivalent plastic strain. Element size and erosion strain have an influence on the response of concrete struck by a high-velocity projectile [61]. Xu et al. [61] did a numerical study where the residual velocity increased with decreasing mesh size, which tells that the mesh size has to be small enough to fit together with the experimental results. The element failure occurs when the equivalent plastic strain is equal to or larger than the erosion strain [61].

Friction is a parameter that helps to provide a realistic description of a penetrating projectile in a ballistic impact test. Here, the friction between the concrete and the penetrating projectile slows down the speed of the projectile, which decreases the residual velocity [70]. The function of friction for ballistic impact situations is studied in the research paper by Khazraiyan et al. [70]. Here, the experiments by Hanchak et al. [39] constitute the reference model, and the original Holmquist-Johnson-Cook model was applied as the material model of concrete.

By taking the friction factor into account, the experimental result is sufficiently rendered. The aspect of friction is considered in the calculation of the opposing force when the projectile is penetrating the concrete slab. A comparison between the experimental data

by Hanchak et al. [39] and different friction coefficients for concrete quality C48 in [70] is shown in Table 3.

Table 3: Effect of friction coefficient on residual velocity by impact of rigid projectile on C48 concrete [70].

Impact velocity (m/s)	Experimental data	Simulated residual velocity (m/s)		
		μ = 0.0	μ = 0.01	μ = 0.02
270	0	0	0	0
301	0	0	0	0
360	67	109	85	71
381	136	156	139	123
434	214	251	238	226
500	315	337	330	321
606	449	463	457	451
746	605	623	617	613
800	670	682	678	674

Friction factor with the value $\mu = 0.02$ gives the smallest difference in velocity when comparing experimental data and simulated data. This shows the effect of implementing the friction factor in the simulation of ballistic impact [70]. The friction on the projectile shank is usually excluded in the penetration analysis due to the difficulties in measuring the pressure and frictional coefficient. The detailed pressure or coefficient is hard to determine, but it is possible to evaluate an approximated amount through experiments. The friction cannot be ignored due to the relatively sizeable effecting area, especially for deep penetration of concrete where the friction will be affecting through the penetration process with more proportion of penetration resistance [71]. In the numerical simulation, the friction is modeled in ABAQUS as a penalty method, including contact between the outer surface of the projectile and the internal and external nodes of the target. The penalty method is used to enforce contact constrains in the normal direction. It reduces the CPU time and memory, and thereby the total amount of cost. As a constraint enforcement method, the penalty method is a stiff approximation of hard contact [72], which is relevant in the analysis of ballistic impact.

Chapter 3 - Method

The primary method used in this thesis is experimental. The experimental method is a part of the scientific method. The scientific method is inductive-deductive, which means that it involves a constant interplay between the concrete (e.g., a specific problem) and the abstract (e.g., scientific or mathematical theory) [73]. It starts with an investigation of a concrete problem which proposes a theoretical explanation for the problem. The theory guides to possible solutions with appropriate data, and analyze them with different models, and then interpret the results to test the possible solutions. If the data confirms the solution, then the process will end. Otherwise, the researcher changes the theory to propose alternative solutions so the process can continue [73]. The three primary methods for collecting data are retrospective studies (historical data), observational studies, and designed experiments [73]. Retrospective studies use previously collected data, observational studies are planned and proactive methods for collecting data, and designed experiments are quite like observational studies, but designed experiments intentionally disturb the process and then observe the results [73]. Disturbing the process allows the experimenter to see what happens when the process or product operates differently from its normal range of conditions [73]. An example of experimental study is the characterization of a product and how to make products robust to known sources of variability [73], which in this case could be related to the dynamic loads on concrete plates.

There are several methods possible to use in the field of ballistic impact. Experimental, numerical, theoretical and analytical considerations are the most used [2, 74]. Experiments of impact problems require practical work with preparation and time that goes into execution. The purpose of conducting experimental work is to be able to predict phenomena, which is essential to society. It helps us to improve the general knowledge, which in this case is useful to build protective structures. The experimentation can be divided into theory-driven experimentation and exploratory experimentation. Theory driven is focusing on various kinds of fact-gathering, such as determining numerical parameters [75]. The exploratory experiment is informed by theory in different ways, and therefore not theory-free. Exploratory experiment phenomena are investigated without first limiting the possible outcomes of the experiment based on an extant theory about the phenomena [75]. The conducted experiments in this thesis focus on exploratory, but the

theory driven will be relevant if it comes to numerical simulation as a method. Numerical simulation is a computer method used in performing science, and the method needs to be subjected to tests of verification and validation to have confidence in the results [75]. From a numerical simulation, it is possible to retrieve information which is very difficult to obtain from experiments. Examples of this are interface forces, thermal effects, stress and strain distributions etc.

The different methods have advantages and disadvantages. One procedure will not always provide all the information from a complex impact phenomenon, so a combination of the different methods is often the best approach. However, a successful application of these methods requires an in-depth understanding of the basic principles. These principles include conservation laws, the role of wave propagation, the influence of inertia and an understanding of material behavior under high rates of loading [20].

3.1 Ballistic impact test

For this thesis, the setup of execution is explained along with an overview of the results from the experiments. The pictures shown in this section are taken at SIMLab. The ballistic impact tests were performed at the SIMLab compressed gas gun facility for concrete compressive strengths of C35, C75 and C110. The concrete is delivered by Unicon, which is one of the leading suppliers in Norway. The concrete certificate note ensures quality with information about the content of the concrete. The recipe for each of the three concrete types is shown in Appendix A – Concrete receipts. The recipes show that an increased level of silica fume is used for an increased level of concrete strength. The w/c ratio is decreasing as the concrete strength increases. For C35, the w/c ratio is 0.55; for C75, the w/c ratio is 0.370, and for C110, the w/c ratio is 0.249. Another vital thing to observe is the increase in density as the compressive strength increases. The C110 is defined as high-performance concrete [76] with a compressive strength of 110 MPa. The test facility gives a great opportunity to study and learn more about the ballistic impact mechanisms in concrete.

3.1.1 Set up and execution

For the C35 plates, the experiments were executed 34 days after casting. The C75 plates were tested 30 days after casting. The concrete plates of C110 were tested 44 days after casting. Some more plates were tested at a later occasion; when the C35 concrete plates

had cured for 58 days and the C75 concrete plates had cured for 51 days. The strength development with curing time must be considered during the analysis. Concrete keeps increasing its strength after 28 days but at a slower level. To minimize error sources, the experiments should have been conducted at the same amount of days after casting for all the concrete plates. The experiments had to be conducted on different days due to practical reasons as a lack of time and resources. The increase of strength was more severe for C35 from day 28 to day 90, compared to C75. One plausible reason for that stronger long-time development could be a higher w/c ratio for the C35, where more water is available for the cement to react with. In total, ten C35 plates, nine C75 plates, and eight C110 plates were tested. Every conducted experiment was not successfully executed, and these results were not taken into further analysis.

Ogival steel projectiles with geometry, as shown in Figure 15, were used in the experiments.

Figure 15: CRH3 ogival projectile


Figure 16: Projectile and sabot

The gas gun is capable of firing 250 g sabots with projectiles installed at a maximum velocity of 1000 m/s when helium is used as a propellant [74]. In this experiment, air is used as a propellant. The use of air gives a maximum projectile velocity of 343 m/s, which is the maximum particle speed in air. Ogival projectiles with CRH3, and a mass of 195 g, are placed in indented sabots that are 3D printed at NTNU, depicted in Figure 16. The sabot has a shape that fits into the barrel, and it is placed in the firing end of the barrel. The sabot is used to fire projectiles smaller than the diameter of the barrel, where the sabot loosens after firing, and the projectile flies freely towards the target.

The pressure tank and the firing unit are filled to predefined pressures to be able to launch the sabot and the projectile. The firing unit is vented to atmospheric pressure when the

pressure chamber reaches the predefined pressure. This makes a pressure gradient equal to the pressure in the tank occur, and the membranes fail. Thus, the projectile and sabot are accelerated. The acceleration keeps increasing during the entire movement through the barrel. The projectile and sabot are separated due to aerodynamic forces. The sabot is prevented from continuing because of a sabot trap placed 1.5 m before the entry of the chamber, which causes the projectile to proceed unobstructed. The location of the sabot trap is where a trigger gets initiated. The trigger initiates flash and sampling from two Phantom v1610 high-speed cameras located on the outside of the chamber. The high-speed cameras have insight into the chamber through a window. The calibration of the cameras before execution is essential to make them capable of tracking the projectile movement through a short interval before and after perforation of the concrete plate. The cameras sample 50.000 frames per second, making it possible to determine the initial and residual velocity of the projectile accurately. When the projectile has perforated the concrete plate, it flies freely into a rag-box filled with graded plywood where it gets stopped.

Figure 17: Compressed gas gun facility at NTNU

Figure 18: Overview of the pressure tank, barrel and the closed impact chamber.

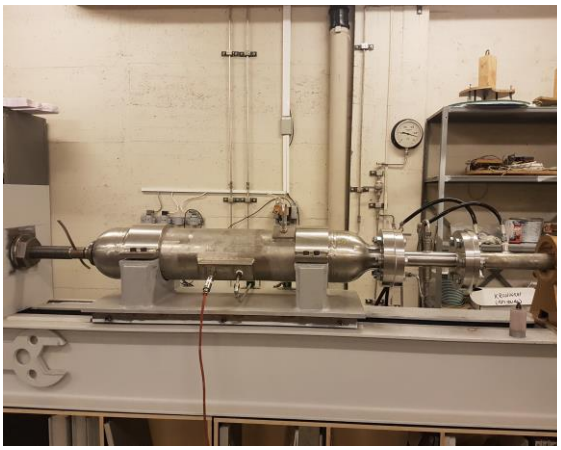

Figure 19: Side view of the pressure tank and firing section.

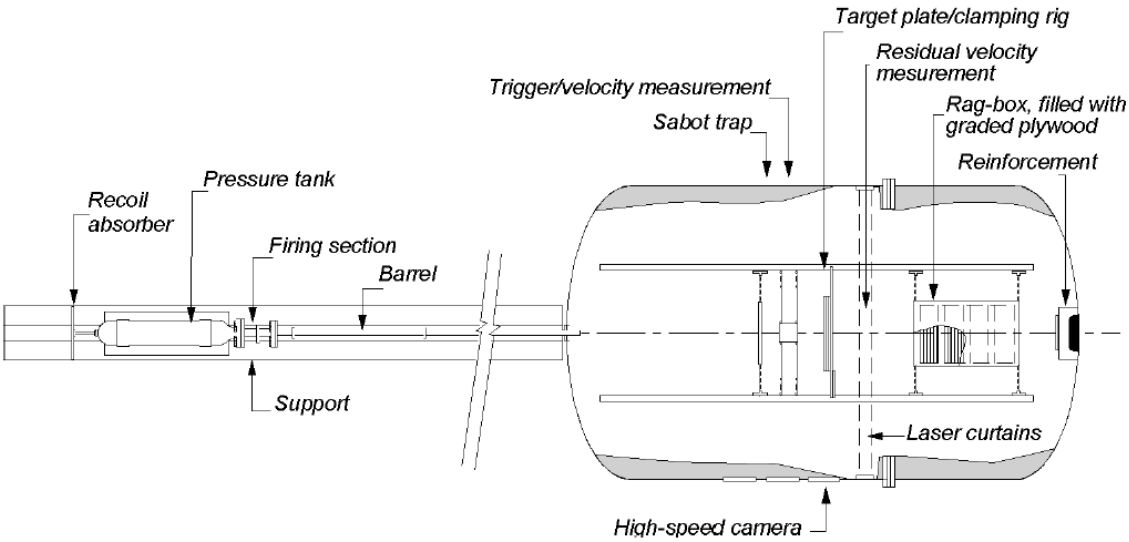

Figure 20: Sketch of compressed gas gun used under ballistic impact test [77].

The target plates have a dimension of 625 × 625 × 50 mm. The plate is hit by the projectile in the center of the plate. Different impact velocities can be obtained by regulating the pressure in the tank. The ballistic limit curve was determined after a series of experiments on the concrete plates. The projectiles and plates were weighed before and after the experiment to obtain the mass loss from projectile perforation, spalling and scabbing of the concrete plate.

The projectile will, in some cases, have a pitch angle before hitting the concrete plate. The critical part is before perforation, where a high pitch angle may significantly reduce the penetration capacity of the striker and must be taken into consideration. However, as the pitch angle is smaller than 5° it can be neglected [20]. Figure 21 shows that the projectile changes direction after perforation tilting downwards. One camera recorded the

front side of the plate, and another camera recorded the rear side of the plate. The first two pictures to the left are showing the frames before perforation of the concrete plate, and the last three pictures to the right are showing the frames after perforation of the concrete plate. The perforation of concrete is a complex process making it hard to predict the exact response.

Figure 21: Time-lapse showing the ballistic impact experiment

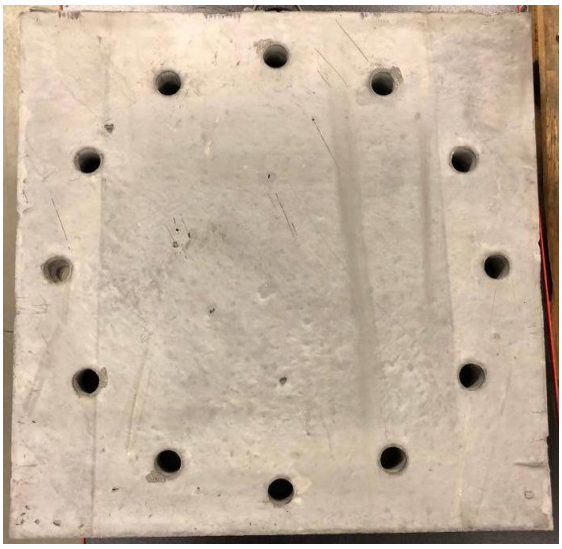

Figure 22: Unperforated concrete plate.

Figure 23: Perforated concrete plates.

Chapter 4 - Analysis

This chapter explains the analysis performed to understand the ballistic impact performance from steel projectiles fired at concrete plates. The pictures shown in this section are taken at SIMLab. The experimental results are presented, and calculations are performed to determine the ballistic limit curve and the ballistic limit velocity for each of the concrete compressive strengths. The experiments and the analytical/empirical models have a connection to each other because the experimental results are used to validate the results from these models.

The analytical analysis will consider the use of the Recht-Ipson model to curve-fit the results from the experiments. This model can predict the time-histories of penetration, velocity and deceleration (load) and values of parameters to be determined by experiments. The CEA-EDF perforation limit formula is used to calculate the ballistic limit velocities. These models are not able to predict the details of failure patterns in concrete targets, this includes size and depth of both impact and scabbing craters, crack initiation, propagation and distribution. There are also more uncertain factors such as aggregate size, distribution, gradation and shape which will complicate the analytical study on concrete penetration and perforation [61].

4.1 Results from the experiments

The results from the experiments are shown in three tables for each of the three concrete compressive strengths: C35, C75 and C110. The tables contain test numbers, initial pressures, initial velocities (v_i), residual velocities (v_r) and mass loss (ΔM) of each plate due to perforation. Some of the results from the experiments are not taken into further analysis due to error, and those results are colored in pink and have comments attached to them.

Table 4: Ballistic impact test on C35.

Test	Pressure	v_i	v_r	ΔM	Comment
	[Bar]	[m/s]	[m/s]	[kg]	
12	9.3	206.4	122.1	-	Plate not weighed before shooting
11	7.0	185.0	104.2	0.4	
10	5.4	-	-	0.9	Came in crookedly
9	5.4	155.3	55.3	0.5	
8	15.0	245.0	173.1	0.3	
7	4.4	143.0		0.5	Hard to see if it went through
6	24.0	294.3	219.3	0.7	
5	4.0	137.7	44.8	0.4	
4	3.6	-	-	0.4	Camera not triggered
2	3.4	119.7	0.0	0.4	Projectile stuck in the plate

Table 5: Ballistic impact test on C75.

Test	Pressure	v_i	v_r	ΔM	Comment
	[Bar]	[m/s]	[m/s]	[kg]	
12	9.3	206.6	115.0	0.3	
11	6.0	170.2	68.1	0.6	
10	24.0	297.9	229.1	0.4	
9	4.0	140.4	0.0	0.5	Hard to see if projectile went through
8	15.0	253.4	170.3	0.8	
7	5.0	157.1	46.2	1.1	
6	4.4	145.6	-	0.5	Hard to see if projectile went through
5	3.0	117.5	0.0	0.6	
4	3.8	131.6	24.2	0.8	

Table 6: Ballistic impact test on C110.

Test	Pressure	v_i	v_r	ΔM	Comment
	[Bar]	[m/s]	[m/s]	[kg]	
8	5.5	155.9	27.2	1	
7	5.0	152.6	0.0	0.8	
6	6.0	163.7	14.3	1.6	
5	7.0	181.9	50.9	1.1	
4	25.0	302.7	208.9	1	
3	15.0	252.9	151.6	1	
2	9.3	205.8	82.4	1.2	
1	5.0	153.6	43.3	0.3	

Based on the results it seems like the mass loss of the concrete plates are generally higher for the lowest velocities. Higher velocity leads to a quicker perforation and less mass loss in form of spalling and scabbing.

Figure 24: Spalling from test 6 with concrete C110

Figure 25: Scabbing from test 6 with concrete C110

The plates showed both spalling and scabbing, and the volume of spalling in the front was less than the volume of scabbing in the rear end of the plate. The size of the craters appears to decrease with increasing initial velocity. Lower impact velocities appear to be more detrimental, because higher impact velocities tend to give more local mechanisms where the failure in the concrete plate goes from flexural bending for low velocities to local/shear for higher velocities. The fragments were larger for lower impact velocities. However, based on the data given in Table 4, Table 5 and Table 6, it is essential to emphasize that there seems to be no clear relation between velocity and mass loss.

There has not been observed a significant effect of increased compressive strength, considering the ballistic resistance. That is in accordance with several studies in the field, concluding that an increase in concrete strength is not reflected in the increase of the ballistic limit velocity [37, 39].

4.2 Damage of plates

The rear side of the plates are shown as the projectiles perforate the plates in Figure 26, Figure 27 and Figure 28. The high-speed camera takes high-quality video, which is used

to perform slow-motion analysis of the fragmentation and velocities before and after the perforation.

Figure 26: Projectile exiting C35 concrete plate for initial velocity from top left corner: 119.7 m/s, 137.7 m/s, 143.0 m/s, 155.3 m/s, 185.0 m/s, 206.4 m/s, 245.0 m/s, 294.3 m/s.

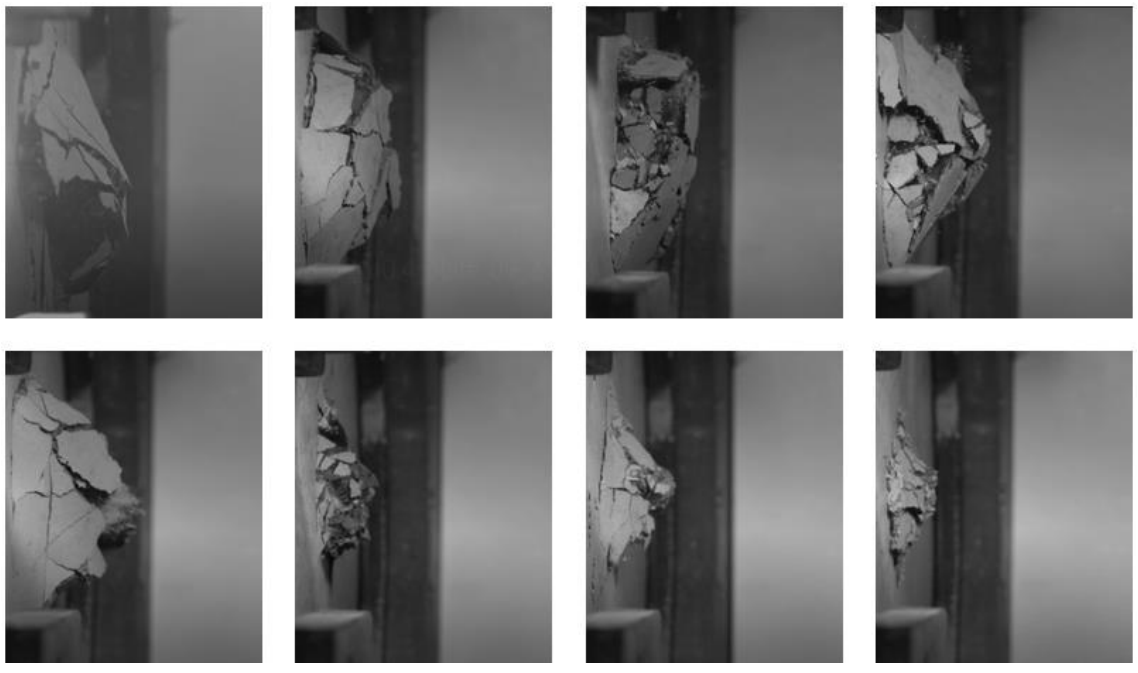

Figure 27: Projectile exiting C75 concrete plate for initial velocity from top left corner: 131.6 m/s, 140.4 m/s, 145.6 m/s, 157.1 m/s, 170.2 m/s, 206.6 m/s, 253.4 m/s, 297.9 m/s.

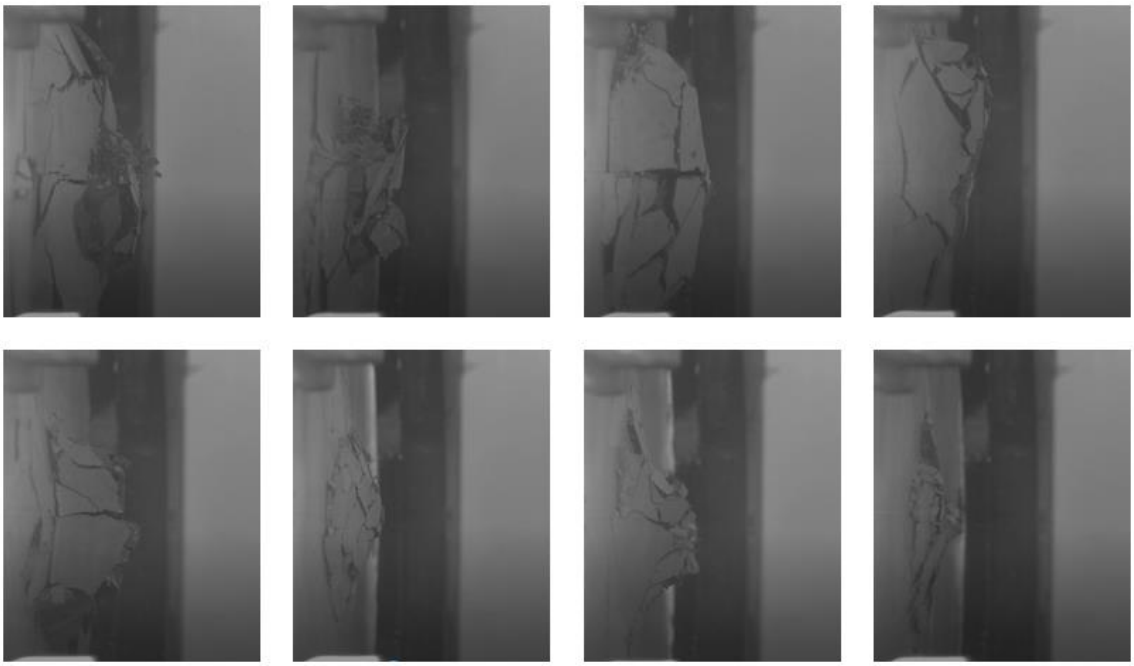

Figure 28: Projectile exiting C110 concrete plate for initial velocity from top left corner: 152.6 m/s, 153.6 m/s, 155.9 m/s, 163.7 m/s, 181.9 m/s, 205.8 m/s, 252.9 m/s, 302.7 m/s.

The pictures are sorted by impact velocity to easily see the damage development of the rear side as the velocity increases. From the figures, there seems to be a tendency that the rear side crater decreases with increasing impact velocity. It looks like lower impact velocities generate larger pieces that loosen from the rear surface. The highest concrete compressive strength of C110 also seems to generate larger pieces that loosen from the rear surface compared to the lowest concrete compressive strength of C35. However, these patterns are not always consistent and rather coincidental, which is rational thinking of the concrete's inhomogeneous properties. The distribution of the different materials in concrete makes it harder to predict, and therefore no clear relation between initial velocity and fragment size could be found.

4.3 Ballistic limit curves

Ballistic limit curves are made from the experimental results. The lowest point in the curve is the ballistic limit velocity, which is the velocity required for a projectile to penetrate a piece of material with a reliability of at least 50% [78]. For example, if 10 test specimens are tested against a specific velocity, and 6 of them are perforated, then it could be counted for as a ballistic limit. A practical explanation is that a given projectile generally will not pierce a specific target when the velocity is lower than the ballistic limit. The term is used mainly in the context of armor, which in this case is a concrete

plate. The ballistic limit v_{bl} of the target is calculated by solving the average of the highest velocity giving partial penetration and the lowest velocity giving complete perforation [3]. The ballistic limit velocity is calculated with the experimental results for each of the three compressive strengths.

C35

$$v_{bl} = \frac{119.7\ m/s + 137.7\ m/s}{2} = 128.7\ m/s$$

C75

$$v_{bl} = \frac{117.5\ m/s + 131.6\ m/s}{2} = 124.6\ m/s$$

C110

$$v_{bl} = \frac{152.6\ m/s + 153.6\ m/s}{2} = 153.1\ m/s$$

The ballistic limit is lower for C75 compared to C35, which is an unexpected result. However, because concrete is a complex material consisting of different elements, the behavior may give an outcome that is unpredictable in some cases. From the experimental results, there are some unexpected values presented, which can be explained by the concrete material properties and the fired steel projectile considering impact velocity and impact angle.

The ballistic limit increases by approximately 16% when the compressive strength of concrete increases from C35 to C110 based on the following calculation:

$$\left(1 - \frac{128.7\ m/s}{153.1\ m/s}\right) \cdot 100\% = 15.94\ m/s \approx 16\ m/s$$

The experimental results are curve fitted to the generalized Recht-Ipson model, referred to in the subsection "2.2.2 Recht-Ipson model", where a, p and v_{bl} are treated as material parameters. The Recht-Ipson model was initially developed for ductile materials, but the generalization of it makes it applicable for concrete as well. Suitable values for a, p and v_{bl} could be found by the least-squares method and the problem solver in Excel. The constant a is used to adjust the height of the curve, meaning that a higher constant gives a steeper curve. The constant p is a parameter used to define how curvy the diagram should be. A high value makes it more curved, while a low value makes it straighter. The

final constant v_{bl} defines the starting point of the curve in the x-axis (initial velocity) representing the ballistic limit velocity. This work aims to adjust the three parameters and curve fit against the obtained results from the experiments. Different methods need to be tested to find a curve that seems to look reasonable and fits the experimental data adequately.

Table 7: Calibrated parameters for the Recht-Ipson model from experimental data.

	a	p	v_{bl}
C35	0.879	1.693	128.7
C75	0.824	1.695	124.6
C110	0.825	1.696	153.1

4.3.1 Ballistic limit curve for C35

The experiments on C35 plates gave seven satisfying results, which could be plotted into a graph. The ballistic limit velocity for this case is 128.7 m/s. The Recht-Ipson model is curve fitted to the graph from the least-squares method used on the experimental results. The Recht-Ipson curve follows the experimental plots in a relatively precise way. The plots deviate a little bit from the Recht-Ipson curve.

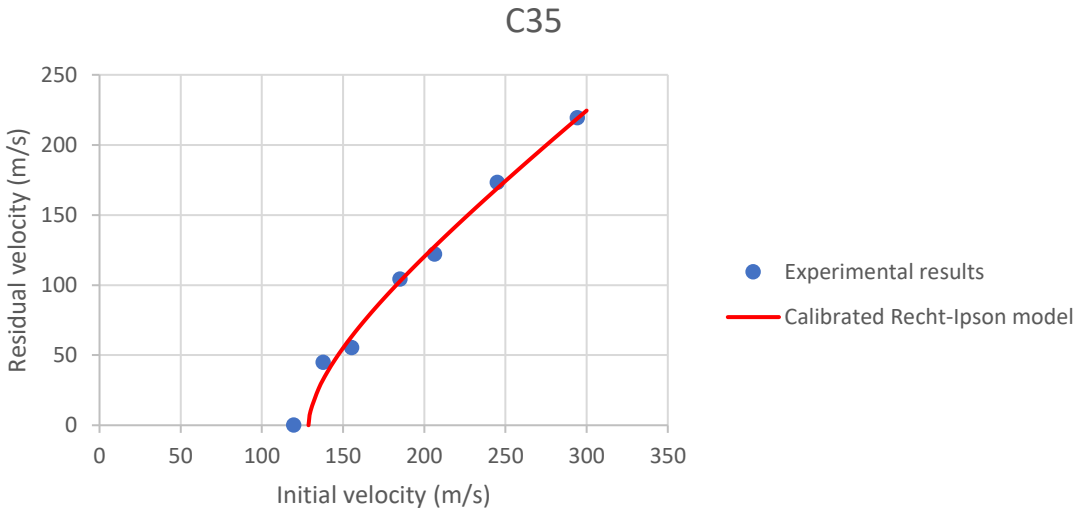

Figure 29: Ballistic limit curve for C35

CEA-EDF perforation limit formula mentioned in subchapter "2.2.3 CEA-EDF perforation limit formula" for calculation of ballistic limit:

$$V_p = 1.3\rho^{\frac{1}{6}} f_c^{\frac{1}{2}} \left(\frac{dH_0^2}{m}\right)^{\frac{2}{3}}$$

As mentioned earlier, this formula is valid for the projectile incident velocities in the range of 20 – 200 m/s and cube compressive strength between 18 – 46 MPa. Each parameter contains these values:

$\rho = 2467\ kg/m^3$, $f_c = 47.2\ MPa = 47.2 \cdot 10^6\ N/m^2$, $d = 0.020\ m$, $H_0 = 0.05\ m$, $m = 0.195\ kg$

The calculation will be

$$V_p = 1.3 \cdot 2467^{\frac{1}{6}} \cdot 47.2 \cdot 10^{6\frac{1}{2}} \cdot \left(\frac{0.020 \cdot 0.05^2}{0.195}\right)^{\frac{2}{3}}$$

$$V_p = 132.5\ m/s$$

Comparing this result to the ballistic limit velocity from the experiments for C35 shows something interesting. The deviation in percentage is 2.86 %, which is very small, so the formula seems to work as intended for this concrete type with the incident velocities.

Deviation:

$$\left(1 - \frac{128.7\ m/s}{132.5\ m/s}\right) * 100\ \% = 2.86\ \%$$

4.3.2 Ballistic limit curve for C75

The experiments on concrete C75 gave seven satisfying results which could be plotted into a graph. The ballistic limit velocity for this case is 124.6 m/s. The Recht-Ipson curve follows the experimental plots in a close way without significant deviations.

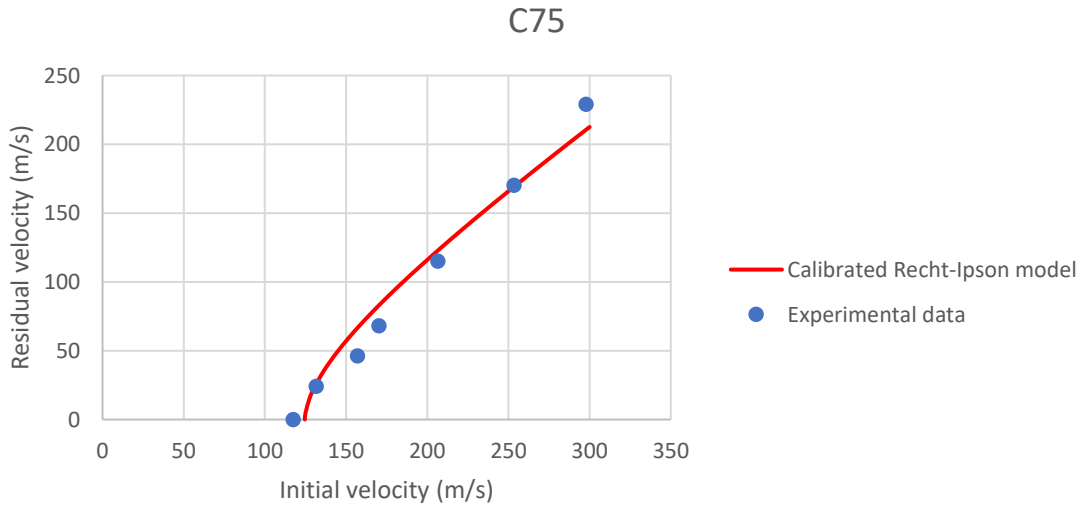

Figure 30: Ballistic limit curve for C75

CEA-EDF perforation limit formula for calculation of ballistic limit:

$$V_p = 1.3\rho^{\frac{1}{6}} f_c^{\frac{1}{2}} \left(\frac{dH_0^2}{m}\right)^{\frac{2}{3}}$$

$\rho = 2509\ kg/m^3$, $f_c = 87.04\ MPa = 87.04 \cdot 10^6\ N/m^2$, $d = 0.020\ m$, $H_0 = 0.05\ m$, $m = 0.195\ kg$

The calculation will be

$$V_p = 1.3 \cdot 2509^{\frac{1}{6}} \cdot 87.04 \cdot 10^{6\frac{1}{2}} \cdot \left(\frac{0.020 \cdot 0.05^2}{0.195}\right)^{\frac{2}{3}}$$

$$V_p = 180.44\ m/s$$

Comparing this result to the ballistic limit velocity from the experiments for C75 shows results as expected. The deviation in percentage is 30,94 %, which is much higher than for C35, so the formula seems to not work for this concrete with the incident velocities.

Deviation:

$$\left(1 - \frac{124.6\ m/s}{180.44\ m/s}\right) * 100\ \% = 30.94\ \%$$

4.3.3 Ballistic limit curve for C110

The experiments on concrete C110 gave eight satisfying results which could be plotted into a graph. The ballistic limit velocity for this case is 153.1 m/s. The Recht-Ipson curve follows the experimental plots in a close way without significant deviations.

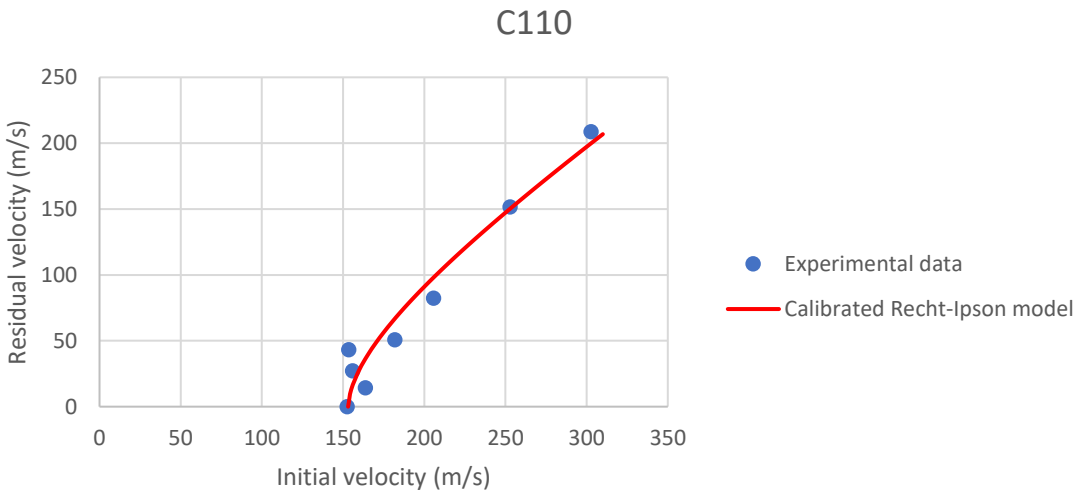

Figure 31: Ballistic limit curve for C110

CEA-EDF perforation limit formula for calculation of ballistic limit:

$$V_p = 1.3\rho^{\frac{1}{6}} f_c^{\frac{1}{2}} \left(\frac{dH_0^2}{m}\right)^{\frac{2}{3}}$$

$\rho = 2555{,}5\ kg/m^3$, $f_c = 118.35\ MPa = 118.35 \cdot 10^6\ N/m^2$, $d = 0.020\ m$, $H_0 = 0.05\ m$, $m = 0.195\ kg$

The calculation will be

$$V_p = 1.3 \cdot 2555.5^{\frac{1}{6}} \cdot 118.35 \cdot 10^{6\frac{1}{2}} \cdot \left(\frac{0.020 \cdot 0.05^2}{0.195}\right)^{\frac{2}{3}}$$

$$V_p = 211\ m/s$$

Comparing this result to the ballistic limit velocity from the experiments for C110 shows results as expected. The deviation in percentage is 27,44 %, which is much higher than for C35, but a little bit lower than for C75. The formula seems to not work for this concrete with the incident velocities.

Deviation:

$$\left(1 - \frac{153{,}1\ m/s}{211\ m/s}\right) * 100\ \% = 27{,}44\ \%$$

Chapter 5 - Ethics

The ethical view of this topic is of common interest. In most cases, the topic is of military interest, and consequentialism will be a central ethical theory. Consequentialism is a part of normative ethics focusing on the ethical action, where it is about evaluating the morality of an action against the outcome of an action. The consequentialism includes many other theories like, for example, utilitarianism, which is about doing the right action based on if it leads to the most positive outcome for the greatest number of people. In another way, it can be formulated that an act is morally right if and only if that act maximizes the good [79]. Consequentialism is a contrast to the deontological ethics [80], which is the normative ethical theory focusing on the morality of an action instead of the consequences of the action. The criticism of consequentialism is often about the negative outcome of an action that produces the most positive outcome for the greatest number of people because some of the people will experience adverse outcomes. It works counter-productive in consequentialist terms where it appears willing to discard or reinterpret intuitive moral judgments in which we have great confidence [81].

Utilitarianism is a paradigm case of consequentialism containing a complex combination of many distinct claims. All these claims can be found from [79]. Most of the claims are logically independent, which makes it possible to accept one claim without accepting others, but the classic utilitarianism accepted all of them. This makes the classic utilitarianism a subject to be attacked in many ways. From a utilitarian perspective, the consequences are all that matters, even though the action itself may be unethical. The right action is the action that creates the most overall happiness [82]. In general, the consequentialists claim that overall utility is the criterion or standard of what is morally right or morally should be done [79]. Utilitarians often discuss that most people in most circumstances should not try to calculate utilities because there is a probability of miscalculating and ending up performing actions that reduce the utility [79].

Chapter 6 - Discussion

A general finding from the experimental results is that an increase in concrete strength is not reflected in the increase of ballistic limit velocity. The increase in concrete strength has a much lower effect than one would expect, where the conducted experiments show that the ballistic limit velocity increases by about 16% when the compressive strength of the concrete increases with a factor of three. For an SFTB, it may be more appropriate to increase the thickness of the concrete rather than increase the compressive strength. Increased thickness will provide better resistance against ballistic impact [83]. However, this is something that needs to be carefully considered in terms of security, but also economical.

No clear correlation was found between mass loss from the projectile impact and impact velocity. There is a tendency of increased mass loss for plain concrete plates when the impact velocity is decreased, and the concrete strength is increased. From a numerical point of view, the main goal of an experiment is to validate numerical results. From an experimental point of view, the main goal is to learn about the phenomenon when a steel projectile strikes a concrete plate. A concrete structure will usually be reinforced, but these plates are not. However, the effect of reinforcement is neglected and believed to be very small based on reports by Hanchak et al. [39].

The generalized Recht-Ipson model to arbitrary projectile nose shape works for ogival steel projectiles fired at concrete plates. The model showed that the ballistic limit curve follows the experimental results by adjusting the three material constants a, p and v_{bl}. These material constants are found from a curve fitting procedure in Excel using the least squares' method. The method of least squares is standard in regression analysis to approximate the solution. It works well for data fitting. The experimental results plotted in an initial versus residual velocity diagram show dots following a pattern. That pattern will be following a curve by applying the least squares method, but the curve is only a best fit based on minimizing the sum of squared residuals, where residuals refers to the difference between the experimental value and the fitted value provided by the model. The least squares curve is then fitted to the Recht-Ipson model.

The CEA-EDF perforation limit formula was used to calculate the ballistic limit velocity, and it worked very accurately for compressive strength of C35, but not for C75 and C110.

The validity of the formula is for incident velocities in the range of 20 – 200 m/s with a cube compression strength between 18 – 46 MPa. The formula gives an estimate of the ballistic limit velocity on plain concrete subjected to hard missile impact. It clearly appears that this empirical model has its limitations with a strict and narrow range of validity.

An assertion based on different nose shapes of projectiles is that the initial velocity is higher when the tip is sharper because it reduces the drag forces. The residual velocity is also affected by the nose shape, where ogival projectiles penetrate the concrete easier than blunt projectiles. The influence of reinforcement and prestressing seem to affect the local and global target deformation as well as penetration resistance. It is essential to know that a 50 mm concrete plate is a thin wall thickness for a securing concrete structure. However, the main purpose of these experiments is not to construct a protective structure but pay attention to the material behavior when subjected to ballistic impact. Another purpose could have been to validate results from numerical simulations as mentioned, and in those cases, the thickness of the plate is not of great importance.

Conservation of energy could be used in penetration modeling, but it is challenging to consider all the different mechanisms that dissipate energy. Also, the proportion of energy dissipation changes with impact velocity. As the impact velocity increases, the projectile kinetic energy is transferred to the target in terms of target kinetic energy and elastic compression energy, where the compression energy dissipates by plastic work later in the process [84]. The transfer of this energy at the time of penetration is what defines the force on the projectile according to work by Walker [85]. Energy rate balance is successful when it includes the transfer of energy stored in the target as elastic compression. This is done automatically within numerical simulations, but not within an analytical model [86]. Conservation of energy could be useful in analytical modeling, but generally over a limited velocity range and projectile-target combination. Recht and Ipson [87] made assumptions on energy dissipation but also submitted the restrictions and range of applicability.

The ballistic impact test can be simulated numerically by using the MHJC model to describe some of the material properties of concrete perforated by projectiles. Unlike the original HJC model, it is found that the MHJC model is a material model that avoids the problem of discontinuity in the normalized equivalent stress area, i.e. when the

normalized pressure is equal to zero. Therefore, the MHJC model gives a more accurate description of the ballistic impact on concrete compared to the original HJC model when no enhancement is applied. The MHJC model is, therefore, more useful to recreate the residual velocity of the projectile from an experiment. The friction coefficient related to the residual velocity is essential in this context because a reasonable friction coefficient is critical to get a lower deviation between the experimental and the numerical results. The friction cannot be ignored, especially for deep penetration concrete targets. The overall friction resistance accounts for a proportion of around 10% in total penetration resistance [71]. A comparison of friction performed on concrete and aluminum-alloy targets perforated by projectiles showed that for the aluminum-alloy target, the increase of penetration depth or impact velocity made the friction coefficient decrease because of the formation of melting layer on the interface between projectile and aluminum-alloy target [71].

In the JH-2 model, the yield strength degrades with damage accumulation, where the JH-1 model operates with a yield strength that degrades when critical damage is reached [65]. The JH-2 material model is more developed compared to the original Holmquist-Johnson model for brittle materials, and therefore it is more efficient to apply on concrete. From research by Oucif et al. [65] it can be understood that the JH-2 model can be used for assessing the impact behavior of plain concrete subjected to high-velocity impact loading. Oucif et al. [88] performed numerical simulation of ballistic penetration and high-velocity impact on plain and reinforced concrete slabs. The damage diameters and residual velocities obtained by JH-2 were compared to the experimental results, which showed good agreement between numerical and experimental results.

Computational methods in the way of numerical simulations are usually time and cost-saving. The expectation for reliable results is getting better over time, and the material models accurately describe the behavior. Even though time and cost probably reduce, it is essential to know the sources of error that may occur in software capable of doing such analysis. It is essential to recognize that it is possible from a numerical simulation to retrieve information that is very difficult to obtain from experiments like internal forces, thermal effects, stress, and strain distributions. An excellent understanding of the fundamental theory of computational mechanics is necessary to succeed.

The need for a knowledge society is a popular topic of political discussion, where research and technology must be a part of the democratic debate about how society should develop [89]. Research is necessary in order to design and produce a new concept as an SFTB. Research ethics is normative related to protecting the fundamental values relevant to research, where scientific research relates to protecting the requirement for truth [89]. The experiments are also seeking the truth by discovering something by observations, where the purpose is to obtain conclusive proof [90]. It is, therefore, essential to secure the quality of the experiments and eliminate the errors that may occur. Uncertainties are commonly referred to as experimental errors, which does not mean that the person conducting the experiments has made a mistake. The word "error" is unfortunate to use as uncertainty based on the fact that the measurement has a limited accuracy [91]. The experimenter has an ethical responsibility to not manipulate the results because manipulation kills the truth. Manipulation of these results may occur in different cases where the ethical judgment is put into a test.

An example is if the politicians who decided to build the coastal highway route require a quick completion of the SFTB. The experimenter has the responsibility of ensuring high quality. In these experiments, it is essential to produce lots of results before concluding, cause few results sometimes make it inexplicable. The time shortage may cause too few results making it hard to conclude, and the experimenter may, in the worst case, manipulate the results to get "good values" making it easier to conclude. This is not good and classified as fraud against good research ethics. Lots of results are not always a good thing, cause more research produces more knowledge, but it also produces more elements of uncertainty. Some of the uncertainties relate to the knowledge itself and how it is produced [92].

Other essential deviating practices needed to be aware of is fabrication, falsification, plagiarism, or other practices that seriously deviate from those that are commonly accepted within the scientific community [93]. Research practice is based on scientific ethos, which is a set of norms and values that govern and regulate research. Scientific ethos is arranged such that it eliminates as many untrue notions as possible and only accepts knowledge if the inherent truth can be proven with solid arguments by looking at e.g., methodology and data [89]. Science is truth-seeking and organized in a way that it produces knowledge. A dynamic network of researchers within the same field contribute

with their insights and perform critical review and validation. Respect for the work of others is important and is done by crediting their work with references. Plagiarism underestimates trust. However, the worst form of aberration is cheating in the form of research fraud, such as fictitious experiments or data [89].

Relevant standards and safety procedures are essential to know before conducting experiments to prevent any damage that may occur. A typical safety issue during laboratory work is the danger of losing heavy objects on your feet. To prevent this, there are safety shoes made to protect from such events. Potentially hazardous events need actions and protective measures. The experimental method is very time consuming as it takes much preparation when it comes to set up and execution. An alternative way to reduce the time is by using a numerical method. The status of numerical simulations as experiments has been examined [94-97]. This literature shows what to learn by such simulations, and the kinds of justification which can be given in applying that knowledge to the "real" world [98, 99]. Vast numbers of calculations can be carried out without requiring direct observation by the experimenter. However, many of these calculations are approximations that introduce uncertainties into the interference from the observation through the simulation [75]. The computer simulations do not seem to belong to either the theoretical or experimental method. Computer simulations seem to involve both aspects with the literature referring to computer simulation as a "third way" for scientific methodology [94], where theoretical reasoning represents the first way, and experimental practice represents the second way. Compared to simulation, the experiment is generally a simulation or idealization of natural conditions without occurring naturally. The problems arise when returning from the idealizations of an experiment to reality and naturally occurring phenomena. Idealization is based on preconceived notions of relevant characteristics of reality, which, in reality, could quickly turn out to be wrong [89].

The experimental work could potentially be a victim of the term "dual-use." The term is used in this case to describe a technology or knowledge that has both civilian and military applications [100]. This project is non-military with an assignment of evaluating the SFTB concept for fragments from internal explosions, e.g., from vehicles transporting dangerous cargo. However, it is a possibility of a terrorist attack. A new innovative concept could be of interest to terrorists to create fear and to ruin something with an economic value [101]. The only thing is that the probability is very small. The researcher

has no control over what happens to experimental results and other findings once they are published. The results can be used by others or refrained from using, which means that they have an ethical responsibility on their own. Sometimes, the research results will be used in contexts that the researcher did not attend, and some may believe that their research results are being misused, which could lead to heated debates in the public arena [89]. This is the disadvantage of having an open source where everyone has access. The researcher has few opportunities to prevent such misuse or to control how the results will be used, and therefore the researcher is not ethically responsible.

Ethical principles can be classified as absolutist and situation based. Absolutist assumes that a set of ethical principles is always valid, while situation based modify or prioritize the ethical principles differently for a situation. Situation based is more realistic, but care has to be taken to ensure that situation based ethics is not used as an excuse to avoid hard ethical issues [102]. This is closely related to consequentialism, where the consequentialist approaches focus on the balance between benefits and harms. Consequentialism theory claims that an act is morally right if that maximizes the good [79]. It is, therefore, essential to make sure that the benefits are higher than the disadvantages. The researcher is responsible for assessing if their research is potentially beneficial for society or not, and the researcher has to be critical when selecting research topics and strategies [103]. Conflict of interest may occur, and the researcher is obliged to be open about possible conflicts of interest. Researchers may be complaisant in creating uncertainty about circumstances that may have influenced the research results based on e.g., their political or religious view.

Several military establishments have research agreements with universities covering a wide range of science and engineering areas [104]. The researchers from the universities must be confident with military work or work that can be used in military applications. Some of the potential scientists may be immigrants from a war-torn country, e.g., Vietnam or Iraq. If they experienced the war with bad memories, then it would be difficult to find a good reason to research military applications. The balance comes into play when the scientist must consider the duty of his work and the research itself which feels morally wrong. Military work is a preparation for an offensive or defensive war, where the scientists who engage in such work should be prepared that their work could be used directly or indirectly in war. In some cases, the legal and ethical obligations can come

into conflict [105], for example, disclosure of secret information restricted by considerations of national security. The viewpoints on the ethics of military work have a wide range, from the belief that military work of any kind is unethical to the belief that military work is a civic duty [106]. From a military perspective, it is a need for defense against outside aggression. However, military work by scientists and engineers tends to increase the disparity of forces and military technology and increase the ability of governments to carry out internal repression [102].

One case is when weapons are produced in one country and sold to another country and later used in war to kill servicemen from the weapons origin country. This happened, for instance, in the Falklands where 255 British servicemen were killed by British weapons [104]. Such changes in an alliance can happen fast, as in the case of Iraq in the Gulf War [102]. Most ethical systems have a ban on taking lives, but this can be limited by other ethical principles that allow the taking of life in certain circumstances, such as self-defense [107]. Military research could be used positively by reducing the destructiveness of war by developing highly accurate weapons. However, the truth is that newer weapons are designed with increasing firepower and destructive capacity which gives the ability to kill a greater number of people in a shorter period of time [102].

The cost of military research is high, which also raises ethical issues. Military spending is expensive and creates generally fewer jobs than other types of expenditure in society [108]. However, dual-use is economically beneficial when considering that expensive military technology could have both military and commercial applications. The problem is if foreign firms take the lead in the commercial development of dual-use technologies, which could make a nation dependent on foreign suppliers for military components [109]. This can potentially threaten national security if foreign suppliers at some point refuse to sell or become enemies.

Military applications may become apparent during the experimental work, where there could potentially be a conflict between responsibilities to sponsors, colleagues and society. It should be tried to avoid undesirable or unethical consequences, e.g., gaining profit from products of publicly funded research, which could be considered unethical. When civilian research funding is limited, the choice may be between accepting military funding with all its ethical questions, or not carrying out the research at all [102].

Chapter 7 - Concluding remarks

The main objective was to investigate the behavior of concrete plates subjected to ballistic impact by steel projectiles. This was done with experimental and analytical/empirical considerations. A numerical literature study was conducted for knowledge of existing numerical simulations. This was done to evaluate different material models applicable to concrete.

The experimental results were interpreted by observations of the projectile movement through the concrete plates. Slow-motion videos from high-speed cameras were used to analyze the perforation process, and the perforation of concrete plates was investigated to assess the damage from an ogival projectile. The ballistic limit curves were produced with the Recht-Ipson analytical model, and the ballistic limit velocity for each concrete compressive strength was calculated with the empirical CEA-EDF perforation formula.

The intention was to investigate different objectives, as referred to in the introduction. The conclusions are structured following the objectives of this thesis:

Objective: To evaluate existing numerical simulations to predict the response of concrete plates subjected to ballistic impact.

- Numerical simulations can predict the residual velocity of the projectiles from the ballistic impact test by using the modified Holmquist-Johnson-Cook model or enhancing the original HJC model. The JH-2 model can also be used and works for assessment of the impact behavior of concrete subjected to high-velocity impact loading. All these material models can provide adequate results compared to the experimental results. It is important to recognize that it is possible to retrieve information from a numerical simulation that is very difficult to obtain from experiments like internal forces, thermal effects, stress and strain distributions. The numerical method is also time and cost-saving compared to the experimental method.

Objective: To investigate how concrete strength affects the ballistic limit.

- Increased concrete strength gives a slightly increased ballistic limit, which means that there is no significant effect of increasing the compressive strength og

concrete when considering the ballistic resistance. It is found from the experiments that an increase from C35 to C110 increases the ballistic limit by approximately 16%.

- The nose shape of the steel projectile plays a critical part on the ballistic limit. Projectiles with a sharp nose shape tend to perforate easier than a blunt nose shape.

Objective: To investigate how the Recht-Ipson model and the CEA-EDF perforation limit formula are used to describe the experimental results.

- The Recht-Ipson model gives a good representation of the experimental results. In order to adjust the curves as accurate as possible, it is crucial to choose the right parameter values for the model.
- The CEA-EDF perforation limit formula worked fine for concrete C35, but not for C75 and C110. The deviation for C35 was 2.86% between the actual and the calculated ballistic limit velocity. Concrete C75 and C110 had deviations of 30.94% and 27.44%, respectively. This confirms that the formula is valid for cube compressive strength between 18 – 46 MPa and incident velocities in the range of 20 – 200 m/s.

Objective: To investigate ethical issues related to the experimental work.

- The researcher has full responsibility when it comes to detecting and eliminating sources of error, ensure the quality of the results and to tell the truth. Plagiarism underestimates the truth with cheating in the form of research fraud as the worst form of aberration, such as fictitious experiments or data. The cost of research evaluated against the utility in society is essential, especially military research generating high expenses. Civilian research projects with interest to the military may cause several ethical issues. Refraining from the research is probably the only way of avoiding any possibility of military applications. Since the issues are complicated, it is not possible to make a statement of what is and is not ethical.

Chapter 8 - Further work

Several interesting investigations are indicated for further work, with the intent to increase a better understanding of this topic.

Concrete structures require reinforcement for improved tensile capacity, and therefore it would be interesting to compare the effect of reinforcement. Concrete plates without reinforcement are not as realistic as with reinforcement. Such experiments should be done to evaluate the effect of reinforcement to ballistic impact, and to obtain a more realistic estimate of the capacity of concrete subjected to these loads.

A similar experiment with same concrete compressive strengths with steel fibers randomly distributed would give some answers on how the concrete behaves when the ductility of the material is increased. It is assumed that this will have a positive effect on the bending of the concrete plate during blast pressure. The effect of fibers on concrete plates subjected to ballistic impact is more difficult to assume but still interesting to investigate.

Another kind of experiment related to fibers that could be performed is the testing of different fiber types, such as glass, nylon, polymer and steel. A comparison of these will give valuable information on what effect a specific type has on concrete exposed to extreme loads.

To conduct a parameter study for ballistic impact with original and modified HJC model, with an evaluation of parameter values, e.g., mesh sensitivity, maximum principal strain at failure, etc.

It is desirable to use a numerical method for further work to compare experimental, analytical and numerical methods.

Bibliography

[1] A. Minoretti, A. Myhr, S. Haugerud, J. Sekse, and T. Fjell Egeberg, "The submerged floating tube bridge: The invisible bridge crossing the Bjørnafjord," in *19th Congress of IABSE*, 2016.

[2] M. Kristoffersen, A. Minoretti, and T. Børvik, "On the internal blast loading of submerged floating tunnels in concrete with circular and rectangular cross-sections," *Engineering Failure Analysis*, vol. 103, pp. 462-480, 2019/09/01/ 2019.

[3] M. E. Backman and W. Goldsmith, "The mechanics of penetration of projectiles into targets," *International Journal of Engineering Science*, vol. 16, no. 1, pp. 1-99, 1978.

[4] G. Corbett, S. Reid, and W. Johnson, "Impact loading of plates and shells by free-flying projectiles: a review," *International Journal of Impact Engineering*, vol. 18, no. 2, pp. 141-230, 1996.

[5] C. E. Anderson Jr and S. R. Bodner, "Ballistic impact: the status of analytical and numerical modeling," *International Journal of Impact Engineering*, vol. 7, no. 1, pp. 9-35, 1988.

[6] J. A. Zukas, *High velocity impact dynamics*. Wiley-Interscience, 1990.

[7] S. J. Brown, "Energy release protection for pressurized systems. Part II: Review of studies into impact/terminal ballistics," 1986.

[8] G. Jonas and J. Zukas, "Mechanics of penetration: analysis and experiment," *International Journal of Engineering Science*, vol. 16, no. 11, pp. 879-903, 1978.

[9] P. Shadbolt, R. Corran, and C. Ruiz, "A comparison of plate perforation models in the sub-ordnance impact velocity range," *International Journal of Impact Engineering*, vol. 1, no. 1, pp. 23-49, 1983.

[10] M. Ravid and S. Bodner, "Dynamic perforation of viscoplastic plates by rigid projectiles," *International Journal of Engineering Science*, vol. 21, no. 6, pp. 577-591, 1983.

[11] J. Liss, W. Goldsmith, and J. Kelly, "A phenomenological penetration model of plates," *International Journal of Impact Engineering*, vol. 1, no. 4, pp. 321-341, 1983.

[12] T. Belytschko, "On difficulty levels in non linear finite element analysis of solids," *IACM expressions*, vol. 2, pp. 6-8, 1996.

[13] M. Maage, "Betong: Regelverk, teknologi og utførelse," *Byggenæringens Forlag AS*, 2017.

[14] S. Jacobsen, *Concrete Technology*. 2016.

[15] P. K. Mehta, *Concrete : structure, properties, and materials*. eng. Englewood Cliffs, N.J, 1993.

[16] A. M. Neville, *Properties of concrete*. eng. Harlow, 1995.

[17] *NS-EN 12390-2:2009 Testing hardened concrete - Part : Making and curing specimens for strength tests*, 2009.

[18] A. M. Neville, *Properties of concrete*. Longman London, 1995.

[19] S. Norge, "NS-EN 1992-1-1: 2004+ NA: 2008: Eurokode 2: Prosjektering av betongkonstruksjoner, Del 1-1: Allmenne regler og regler for bygninger," *Brussel: CEN*, 2008.

[20] T. Børvik, O. S. Hopperstad, and M. Langseth, "Impact Mechanics - Part 2: An Introduction to Penetration and Perforation Mechanics," 2016.

[21] M. Zineddin and T. Krauthammer, "Dynamic response and behavior of reinforced concrete slabs under impact loading," *International Journal of Impact Engineering*, vol. 34, no. 9, pp. 1517-1534, 2007.
[22] G. Thiagarajan, A. V. Kadambi, S. Robert, and C. F. Johnson, "Experimental and finite element analysis of doubly reinforced concrete slabs subjected to blast loads," *International Journal of Impact Engineering*, vol. 75, pp. 162-173, 2015.
[23] Y. Tai, T. Chu, H.-T. Hu, and J. Wu, "Dynamic response of a reinforced concrete slab subjected to air blast load," *Theoretical and applied fracture mechanics*, vol. 56, no. 3, pp. 140-147, 2011.
[24] B. Luccioni *et al.*, "Experimental and numerical analysis of blast response of High Strength Fiber Reinforced Concrete slabs," *Engineering Structures*, vol. 175, pp. 113-122, 2018/11/15/ 2018.
[25] O. Algassem, Y. Li, and H. Aoude, "Ability of steel fibers to enhance the shear and flexural behavior of high-strength concrete beams subjected to blast loads," *Engineering Structures*, vol. 199, p. 109611, 2019/11/15/ 2019.
[26] H. Langberg and G. Markeset, "High-Performance Concrete - Penetration Resistance and Material Development," *Proceedings of the 9th International Symposium on Interaction of the Effects of Munitions with Structures*, pp. 299-306, 1999/05/3-7 1999.
[27] H. Aoude, F. P. Dagenais, R. P. Burrell, and M. Saatcioglu, "Behavior of ultra-high performance fiber reinforced concrete columns under blast loading," *International Journal of Impact Engineering*, vol. 80, pp. 185-202, 2015.
[28] Z. S. Tabatabaei, J. S. Volz, J. Baird, B. P. Gliha, and D. I. Keener, "Experimental and numerical analyses of long carbon fiber reinforced concrete panels exposed to blast loading," *International Journal of Impact Engineering*, vol. 57, pp. 70-80, 2013.
[29] D. Li and S. Liu, "The influence of steel fiber on water permeability of concrete under sustained compressive load," *Construction and Building Materials*, vol. 242, p. 118058, 2020/05/10/ 2020.
[30] Y. Zheng, X. Wu, G. He, Q. Shang, J. Xu, and Y. Sun, "Mechanical Properties of Steel Fiber-Reinforced Concrete by Vibratory Mixing Technology," *Advances in Civil Engineering*, vol. 2018, p. 9025715, 2018/07/12 2018.
[31] Vegdirektoratet, "PP-fiber til bruk i brannsikring av betong, produksjon av testelementer for brannprøving," p. 2, 2013.
[32] H.-w. Ye *et al.*, "Research on fire resistance of ultra-high-performance concrete," *Advances in Materials Science and Engineering*, vol. 2012, 2012.
[33] H. Muller and M. Haist, "Bauen im bestand-markt der zukunft-innovative betonbautechniken-potenziale fur die vorfertigung?(building in the context of existing structuresa future market-innovative concrete construction methodsopportunities for prefabrication?)," *Betonwerk und Fertigteil-Technik/Concrete Plant and Precast Technology*, vol. 74, no. 2, pp. 144-145, 2008.
[34] K. Habel, M. Viviani, E. Denarié, and E. Brühwiler, "Development of the mechanical properties of an ultra-high performance fiber reinforced concrete (UHPFRC)," *Cement and Concrete Research*, vol. 36, no. 7, pp. 1362-1370, 2006.
[35] J. Shu, T. Kanstad, M. Hendriks, J. A. Øverli, and A. Barenys, "Structural Performance of Reinforced Concrete Slab Subjected to Fire and Explosion," in *International conference on Interdisciplinary Approaches for Cement-based Materials and Structural Concrete: Synergizing Expertise and Bridging Scales of Space and Time*, 2018, pp. 785-790: Rilem publications.

[36] E. J. Conrath, "Structural design for physical security: State of the practice," 1999: American society of civil engineers.
[37] T. Børvik, O. E. Gjørv, and M. Langseth, "Ballistic Perforation Resistance of High-Strength Concrete Slabs," pp. 61-66, June 2007 2007.
[38] Q. M. Li, S. R. Reid, H. M. Wen, and A. R. Telford, "Local impact effects of hard missiles on concrete targets," *International Journal of Impact Engineering,* vol. 32, no. 1, pp. 224-284, 2005/12/01/ 2005.
[39] S. J. Hanchak, M. J. Forrestal, E. R. Young, and J. Q. Ehrgott, "Perforation of concrete slabs with 48 MPa (7 ksi) and 140 MPa (20 ksi) unconfined compressive strengths," *International Journal of Impact Engineering,* vol. 12, no. 1, pp. 1-7, 1992/01/01/ 1992.
[40] T. Jankowiak, A. Rusinek, and P. Wood, "A numerical analysis of the dynamic behaviour of sheet steel perforated by a conical projectile under ballistic conditions," *Finite Elements in Analysis and Design,* vol. 65, pp. 39-49, 2013/03/01/ 2013.
[41] W. Goldsmith, "Non-ideal projectile impact on targets," *International Journal of Impact Engineering,* vol. 22, no. 2-3, pp. 95-395, 1999.
[42] M. Polanco-Loria, O. Hopperstad, T. Børvik, and T. Berstad, "Numerical predictions of ballistic limits for concrete slabs using a modified version of the HJC concrete model," *International Journal of Impact Engineering,* vol. 35, pp. 290-303, 05/01 2008.
[43] T. J. Holmquist, G. R. Johnson, and W. H. Cook, "A Computational Constitutive Model for Concrete Subjected to Large Strains, High Strain Rates and High Pressures," *14th International symposium on ballistics, Quebec, Canada,* vol. 2, pp. 591-600 1993.
[44] W. Riedel, K. Thoma, S. Hiermaier, and E. Schmolinske, "Penetration of reinforced concrete by BETA-B-500 numerical analysis using a new macroscopic concrete model for hydrocodes," in *Proceedings of the 9th International Symposium on the Effects of Munitions with Structures,* 1999, vol. 315: Berlin-Strausberg Germany.
[45] N. Gebbeken and M. Ruppert, "A new material model for concrete in high-dynamic hydrocode simulations," *Archive of Applied Mechanics,* vol. 70, no. 7, pp. 463-478, 2000.
[46] H. Swift, L. Greszczuk, J. Zukas, T. Nicholas, and D. Curran, "Impact dynamics," ed: New York: John Wiley & Sons, 1982.
[47] A. Rajput and M. A. Iqbal, "Ballistic performance of plain, reinforced and pre-stressed concrete slabs under normal impact by an ogival-nosed projectile," *International Journal of Impact Engineering,* vol. 110, pp. 57-71, 2017/12/01/ 2017.
[48] G. Ben-Dor, A. Dubinsky, and T. Elperin, "Empirical models for predicting protective properties of concrete shields against high-speed impact," *Journal of Mechanics of Materials and Structures,* vol. 8, no. 2, pp. 199-232, 2013.
[49] G. Hughes, "Hard missile impact on reinforced concrete," *Nuclear Engineering and design,* vol. 77, no. 1, pp. 23-35, 1984.
[50] R. Kennedy, "A review of procedures for the analysis and design of concrete structures to resist missile impact effects," *Nuclear Engineering and Design,* vol. 37, no. 2, pp. 183-203, 1976.
[51] Q. Li, S. Reid, H. Wen, and A. Telford, "Local impact effects of hard missiles on concrete targets," *International Journal of impact engineering,* vol. 32, no. 1-4, pp. 224-284, 2005.

[52] A. Rajput, M. A. Iqbal, and N. K. Gupta, "Ballistic performances of concrete targets subjected to long projectile impact," *Thin-Walled Structures,* vol. 126, pp. 171-181, 2018/05/01/ 2018.
[53] M. Forrestal, D. Frew, S. Hanchak, and N. Brar, "Penetration of grout and concrete targets with ogive-nose steel projectiles," *International Journal of Impact Engineering,* vol. 18, no. 5, pp. 465-476, 1996.
[54] Z. Mu and W. Zhang, "An investigation on mass loss of ogival projectiles penetrating concrete targets," *International journal of impact engineering,* vol. 38, no. 8-9, pp. 770-778, 2011.
[55] P. Barr, P. Carter, W. Howe, A. Neilson, and A. Richards, "Experimental studies of the impact resistance of steel faced concrete composites," 1983.
[56] A. Dancygier and D. Yankelevsky, "High strength concrete response to hard projectile impact," *International Journal of Impact Engineering,* vol. 18, no. 6, pp. 583-599, 1996.
[57] Y. D. Zhang, Z. C. Lu, and H. M. Wen, "On the penetration of semi-infinite concrete targets by ogival-nosed projectiles at different velocities," *International Journal of Impact Engineering,* vol. 129, pp. 128-140, 2019/07/01/ 2019.
[58] H. Wen, Y. Yang, and T. He, "Effects of abrasion on the penetration of ogival-nosed projectiles into concrete targets," *Latin American Journal of Solids and Structures,* vol. 7, no. 4, pp. 413-422, 2010.
[59] O. S. Hopperstad and T. Børvik, "Impact Mechanics - Part 1: Modelling of plasticity and failure with explicit finite element methods," 2018.
[60] D. Morin, L. E. B. Dæhli, T. Børvik, A. Benallal, and O. S. Hopperstad, "Numerical study of ductile failure under non-proportional loading," *European Journal of Mechanics-A/Solids,* vol. 74, pp. 221-241, 2019.
[61] L. Xu, H. Xu, and H. Wen, "On the penetration and perforation of concrete targets struck transversely by ogival-nosed projectiles-a numerical study," *International Journal of Impact Engineering,* vol. 125, pp. 39-55, 2019.
[62] G. Johnson and T. Holmquist, "A computational constitutive model for brittle materials subjected to large strains, high strain rates and high pressures," *Shock wave and high-strain-rate phenomena in materials,* pp. 1075-1081, 1992.
[63] G. R. Johnson and T. J. Holmquist, "An improved computational constitutive model for brittle materials," in *AIP Conference Proceedings*, 1994, vol. 309, no. 1, pp. 981-984: American Institute of Physics.
[64] M. Saleh, L. Edwards, and I. G. Crouch, "9 - Numerical modelling and computer simulations," in *The Science of Armour Materials*, I. G. Crouch, Ed.: Woodhead Publishing, 2017, pp. 483-579.
[65] C. Oucif, J. S. Kalyana Rama, K. Shankar Ram, and F. Abed, "Damage modeling of ballistic penetration and impact behavior of concrete panel under low and high velocities," *Defence Technology,* 2020/03/31/ 2020.
[66] H. Xu and H. Wen, "A computational constitutive model for concrete subjected to dynamic loadings," *International Journal of Impact Engineering,* vol. 91, pp. 116-125, 2016.
[67] T. Børvik, S. Dey, and A. Clausen, "Perforation resistance of five different high-strength steel plates subjected to small-arms projectiles," *International Journal of Impact Engineering,* vol. 36, no. 7, pp. 948-964, 2009.
[68] S. Dey, T. Børvik, O. Hopperstad, and M. Langseth, "On the influence of constitutive relation in projectile impact of steel plates," *International Journal of Impact Engineering,* vol. 34, no. 3, pp. 464-486, 2007.

[69] J. K. Holmen, J. K. Solberg, O. S. Hopperstad, and T. Børvik, "Ballistic impact of layered and case-hardened steel plates," *International Journal of Impact Engineering*, vol. 110, pp. 4-14, 2017.
[70] N. Khazraiyan, G. Liaghat, H. Khodarahmi, and N. Dashtian-Gerami, "Analysis of perforation process into concrete/metal targets by rigid projectiles," *Proceedings of the Institution of Mechanical Engineers, Part C: Journal of Mechanical Engineering Science*, vol. 227, no. 7, pp. 1454-1468, 2013.
[71] C. G. Chai, A. G. Pi, Q. M. Li, and F. L. Huang, "On the friction effects on rigid-body penetration in concrete and aluminium-alloy targets," *Defence Technology*, vol. 15, no. 4, pp. 576-581, 2019/08/01/ 2019.
[72] "ABAQUS Analysis User's Manual Version 2019," ed: SIMULIA, 2019.
[73] G. Vining, "Technical advice: Scientific method and approaches for collecting data," *Quality Engineering*, vol. 25, no. 2, pp. 194-201, 2013.
[74] T. Børvik, *Ballistic penetration and perforation of steel plates*. Fakultet for ingeniørvitenskap og teknologi, 2001.
[75] H. Andersen and B. Hepburn, "Scientific method," 2015.
[76] V. Patel and N. Shah, "A survey of high performance concrete developments in civil engineering field," *Open Journal of Civil Engineering*, vol. 3, no. 02, p. 69, 2013.
[77] T. Børvik, M. Langseth, and K. Malo, "A Compressed Gas Gun for Impact Testing," *Norwegian Defence Construction Service*, 1997.
[78] P. J. Hazell, *Armour: materials, theory, and design*. CRC Press, 2015.
[79] W. Sinnott-Armstrong, "Consequentialism," 2003.
[80] L. Alexander and M. Moore, "Deontological ethics," 2007.
[81] S. Scheffler, *Consequentialism and its Critics*. Oxford University Press on Demand, 1988.
[82] J. Driver, "The history of utilitarianism," 2009.
[83] A. Rajput and M. A. Iqbal, "Impact behavior of plain, reinforced and prestressed concrete targets," *Materials & Design*, vol. 114, pp. 459-474, 2017/01/15/ 2017.
[84] C. E. Anderson Jr, D. L. Littlefield, and J. D. Walker, "Long-rod penetration, target resistance, and hypervelocity impact," *International Journal of Impact Engineering*, vol. 14, no. 1-4, pp. 1-12, 1993.
[85] J. D. Walker, "Hypervelocity penetration modeling: momentum vs. energy and energy transfer mechanisms," *International journal of impact engineering*, vol. 26, no. 1-10, pp. 809-822, 2001.
[86] C. E. Anderson Jr, "Analytical models for penetration mechanics: A Review," *International Journal of Impact Engineering*, vol. 108, pp. 3-26, 2017/10/01/ 2017.
[87] R. Recht and T. Ipson, "Ballistic perforation dynamics," 1963.
[88] C. Oucif, L. M. Mauludin, and F. Abed, "Ballistic behavior of plain and reinforced concrete slabs under high velocity impact," *Frontiers of Structural and Civil Engineering*, vol. 14, no. 2, pp. 299-310, 2020/04/01 2020.
[89] M. Kaiser, "Science and technology," *The Norwegian National RESEARCH ETHICS COMMITTEES*, 2015.
[90] J. L. Moreno, *Sociometry, experimental method and the science of society*. Lulu. com, 1951.
[91] R. T. E. Fisher, *Enjoy Writing Your Thesis or Dissertation*. 2014.
[92] W. E. Walker *et al.*, "Defining uncertainty: a conceptual basis for uncertainty management in model-based decision support," *Integrated assessment*, vol. 4, no. 1, pp. 5-17, 2003.

[93] H. K. Schachman, "What is misconduct in science?," *Science,* vol. 261, no. 5118, pp. 148-183, 1993.
[94] W. J. Kaufmann and L. L. Smarr, *Supercomputing and the Transformation of Science*. WH Freeman & Co., 1992.
[95] P. Humphreys, "Computational science and scientific method," *Minds and Machines,* vol. 5, no. 4, pp. 499-512, 1995.
[96] R. I. Hughes, "The Ising model, computer simulation, and universal physics," *Ideas in Context,* vol. 52, pp. 97-145, 1999.
[97] S. Norton and F. Suppe, "Why atmospheric modeling is good science," *Changing the atmosphere: Expert knowledge and environmental governance,* pp. 67-105, 2001.
[98] D. G. Mayo, *Error and the growth of experimental knowledge*. University of Chicago Press, 1996.
[99] W. S. Parker, "Franklin, Holmes, and the epistemology of computer simulation," *International Studies in the Philosophy of Science,* vol. 22, no. 2, pp. 165-183, 2008.
[100] K. D. Haggerty and R. V. Ericson, "The military technostructures of policing," *The Canadian Review of Policing Research,* vol. 1, 2004.
[101] G. S. Becker and Y. Rubinstein, "Fear and the response to terrorism: an economic analysis," *University of Chicago mimeo,* vol. 93, 2004.
[102] M. A. Hersh, "The ethics of military work: A guide for scientists and engineers," *IFAC Proceedings Volumes,* vol. 33, no. 8, pp. 95-106, 2000.
[103] N. C. F. R. E. I. Science and Technology, "Guidelines for Research Ethics in Science and Technology," ed: De nasjonale forskningsetiske komiteer Oslo, 2008.
[104] R. Evans, N. Butler, and E. Gonçalves, *The campus connection: military research on campus*. CND Publications Limited, 1991.
[105] P. Park, "The ethical engineer and the law," *Engineering Science & Education Journal,* vol. 4, no. 6, pp. 277-280, 1995.
[106] K. W. Kemp, "Conducting scientific research for the military as a civic duty," in *Ethical issues in scientific research an anthology*: Garland Publishing Inc., 1994, pp. 387-396.
[107] R. Norman, *Ethics, killing and war*. Cambridge University Press, 1995.
[108] T. Voss, *Converting the defence industry: have we the political will?* (no. 9). Oxford Research Group Oxford, 1992.
[109] J. Stowsky, "The dual-use dilemma," *Issues in Science and Technology,* vol. 13, no. 2, pp. 56-64, 1996.

Appendix A – Concrete receipts

Betonkontrolattest
v. 1.14
side 1 d. 29.03.2019 kl. 09:56

unicon
GEMENTIR HOLDING

Inspec.lot no.: 040010431111 Prod. Id, SKAKO: 2019020620005

Salgsordre	2096664	**Recept**	UN53X-D000
Prod.ordre	106527510		
Debitorkonto	1040977		
	NTNU		
Adresse	Richard Birkelandsvei 1A		
	7034 Trondheim		
	Tore Børvik		
	93059462		
Fabrik	0332 Fossegrenda	**Produceret (m³)**	0,99
Følgeseddel	1986544	**Blandedato**	06.02.2019
		Blandetidspunkt	08:50

Ønsket temperatur	20 °C	
Ønsket konsistens	200	
Blandemester	khgu	
Blander	000	
Vognnr.	825	

Sammensætning	Materialenavn	Fugt %	Densitet kg/m³	Tilsat(bør)	Blandet kg	1 m³(bør)	V.O.T.er
Pulver	Norcem Anlegg FA		3.020	305	308	305	310
Pulver	Silikastøv k=2		2.200	13	13	13	13
Tilslag	0-8 Forset	4,2	2.720	1.124	1.108	1.079	1.069
Tilslag	8-16 Merefstad KF	-0,4	2.870	841	849	845	857
Additiver	MasterGlenium SKY 899	80,0	1.040	1,54	1,55	1,53	1,56
Vand	Kaldt vann		1.000	5			
Vand	Kaldt vann		1.000	33	33	80	33
Vand	Varmt vann		1.000	101	103	101	104
			Total fugt i tilslag				41
			Total kg	2.423	2.416	2.424	2.429
			Volumen (liter)	1.000	994	1.000	1.000

	Bør værdi	Målt / bereg.	
Temperatur	20	17,000	°C
Total vand	182	182,0	1/m3
Ækvivalent cement målt/beregnet	331	330,9	kg/m3
Ækvivalent V/C- forhold målt/beregnet	0,550	0,550	
Konsistens	200	200	mm
Blandetid målt/beregnet	60	282	sec
Målt luftindhold på frisk beton	2,0		%
Wattmeter målt/beregnet	70	78	
Beregning af densitet	2429	2467	kg/m3

	Bør værdi	Målt / bereg.	
Middelverdi 7 døgn MPa		28,830	MPa
Trykprøvning 28 MPa		47,200	MPa
Middelværdi 28 døgn MPa		46,800	MPa
Sylinderfasthet 28 d		36,504	MPa
Densitet 28 døgn [kg/m3]		2467,000	kg/m3

57. C35 serie 1 til NTNU

Figure 32: Receipt of the C35 concrete.

Betonkontrolattest

v. 1.14
side 1 d. 29.03.2019 kl. 09:56

unicon
CEMENTIR HOLDING

Inspec.lot no.: 040010465135 Prod. Id, SKAKO: 2019021220077

Salgsordre	2096665	**Recept**	UN53X-D000		
Prod.ordre	106542351				
Debitorkonto	1040977				
	NTNU			**Ønsket temperatur**	20 ºC
Adresse	Richard Birkelandsvei 1A			**Ønsket konsistens**	200
	7034 Trondheim			**Blandemester**	omv
	Tore Børvik			**Blander**	000
	93059462			**Vognnr.**	831
Fabrik	0332 Fossegrenda	**Produceret (m³)**	0,98		
Følgeseddel	1986724	**Blandedato**	12.02.2019		
		Blandetidspunkt	09:12		

Sammensætning	Materialenavn	Fugt %	Densitet kg/m³	Tilsat(bør)	Blandet kg	1 m³(bør)	V.O.T.er
Pulver	Norcem Anlegg FA		3.020	427	425	427	435
Pulver	Silika ikke med i V/C		2.200	10	10	10	11
Pulver	Silikastøv k=1		2.200	38	39	38	39
Tilslag	0-8 Forset	4,3	2.720	957	932	917	914
Tilslag	8-16 Merefstad KF	-0,2	2.870	879	872	881	893
Additiver	MasterGlenium SKY 899	80,0	1.040	4,06	4,04	4,06	4,13
Vand	Kaldt vann		1.000	10	1		1
Vand	Kaldt vann		1.000	20	18	67	18
Vand	Varmt vann		1.000	101	103	101	105
			Total fugt i tilslag				38
			Total kg	2.446	2.404	2.446	2.458
			Volumen (liter)	1.000	978	1.000	1.000

	Bør værdi	Målt / bereg.	
Temperatur	20	19,200	°C
Total vand	172	172,0	1/m3
Ækvivalent cement målt/beregnet	465	464,9	kg/m3
Ækvivalent V/C- forhold målt/beregnet	0,370	0,370	
Konsistens	200	220	mm
Blandetid målt/beregnet	60	193	sec
Målt luftindhold på frisk beton	2,0		%
Wattmeter målt/beregnet	70	121	
Beregning af densitet	2458	2502	kg/m3

	Bør værdi	Målt / bereg.	
Middelverdi 7 døgn MPa		60,420	MPa
Trykprøvning 28 MPa		87,040	MPa
Middelværdi 28 døgn MPa		87,155	MPa
Sylinderfasthet 28 d		71,467	MPa
Densitet 28 døgn [kg/m3]		2509,000	kg/m3

66. SU= 360. C75 serie 1

Figure 33: Receipt of the C75 concrete.

Betonkontrolattest

v. 1.14
side 1 d. 29.03.2019 kl. 09:56

unicon
CEMENTIR HOLDING

Inspec.lot no.: 040010490695 Prod. Id, SKAKO: 2019021920026

Salgsordre	2096667	**Recept**	UN53X-D000		
Prod.ordre	106561255				
Debitorkonto	1040977				
	NTNU			**Ønsket temperatur**	20 °C
Adresse	Richard Birkelandsvei 1A			**Ønsket konsistens**	200
	7034 Trondheim			**Blandemester**	halo
	Tore Børvik			**Blander**	000
	93059462			**Vognnr.**	863
Fabrik	0332 Fossegrenda	**Produceret (m³)**	0,99		
Følgeseddel	1986974	**Blandedato**	19.02.2019		
		Blandetidspunkt	08:46		

Sammensætning	Materialenavn	Fugt %	Densitet kg/m³	Tilsat(bør)	Blandet kg	1 m³(bør)	V.O.T.er
Pulver	Norcem Anlegg FA		3.020	536	535	536	540
Pulver	Silika ikke med i V/C		2.200	45	46	45	46
Pulver	Silikastøv k=1		2.200	58	58	58	59
Tilslag	0-8 Forset	4,3	2.720	893	876	857	847
Tilslag	8-16 Merefstad KF		2.870	835	846	835	853
Additiver	MasterGlenium SKY 899	80,0	1.040	10,74	10,68	10,73	10,77
Vand	Kaldt vann		1.000	10	4		4
Vand	Kaldt vann		1.000	15	14	62	14
Vand	Varmt vann		1.000	78	79	78	80
			Total fugt i tilslag				36
			Total kg	2.481	2.469	2.481	2.491
			Volumen (liter)	1.000	991	1.000	1.000

	Bør værdi	Målt / bereg.	
Temperatur	20	20,400	°C
Total vand	148	148,0	1/m3
Ækvivalent cement målt/beregnet	594	594,4	kg/m3
Ækvivalent V/C- forhold målt/beregnet	0,249	0,249	
Konsistens	200	250	mm
Blandetid målt/beregnet	60	419	sec
Målt luftindhold på frisk beton	2,0		%
Wattmeter målt/beregnet	70	231	
Beregning af densitet	2491	2554	kg/m3

	Bør værdi	Målt / bereg.	
Middelverdi 7 døgn MPa		91,250	MPa
Trykprøvning 28 MPa		118,350	MPa
Middelværdi 28 døgn MPa		119,775	MPa
Sylinderfasthet 28 d		98,216	MPa
Densitet 28 døgn [kg/m3]		2555,500	kg/m3

78. C110 NTNU serie 1

Figure 34: Receipt of the C110 concrete.